energies

MDPI

Article

A Distributed Cooperative Anti-Windup Algorithm Improving Voltage Profile in Distribution Systems with DERs' Reactive Power Saturation

Giovanni Mercurio Casolino, Giuseppe Fusco * and Mario Russo

Department of Electrical and Information Engineering, University of Cassino and Southern Lazio, Via G. Di Biasio 43, 03043 Cassino, Italy; casolino@unicas.it (G.M.C.); russo@unicas.it (M.R.)
* Correspondence: fusco@unicas.it

Abstract

This paper proposes a Distributed Cooperative Algorithm (DCA) that solves the windup problem caused by the saturation of the Distributed Energy Resource (DER) PI-based control unit. If the reference reactive current output by the PI exceeds the maximum reactive power capacity of the DER, the control unit saturates, preventing the optimal voltage regulation at the connection node of the Active Distribution Network (ADN). Instead of relying on a centralized solution, we proposed a cooperative approach in which each DER's control unit takes part in the DCA. If a control unit saturates, the voltage regulation error is not null, and the algorithm is activated to assign a share of this error to all DERs' control units according to a weighted average principle. Subsequently, the algorithm determines the control unit's new value of the voltage setpoint, desaturating the DER and enhancing the voltage profile. The proposed DCA is independent of the design of the control unit, does not require parameter tuning, exchanges only the regulation error at a low sampling rate, handles multiple saturations, and has limited communication requirements. The effectiveness of the proposed DCA is validated through numerical simulations of an ADN composed of two IEEE 13-bus Test Feeders.

Keywords: anti-windup; control of renewable energy resources; decentralized and distributed control; output regulation; smart grids; systems with saturation

Academic Editors: Jacob G. Fantidis and Antonis Tsikalakis

Received: 6 June 2025
Revised: 30 June 2025
Accepted: 1 July 2025
Published: 4 July 2025

Citation: Casolino, G.M.; Fusco, G.; Russo, M. A Distributed Cooperative Anti-Windup Algorithm Improving Voltage Profile in Distribution Systems with DERs' Reactive Power Saturation. *Energies* **2025**, *18*, 3540. https://doi.org/10.3390/en18133540

1. Introduction

Distribution networks are becoming active systems because many Distributed Energy Resources (DERs) are being connected. DERs include distributed generation, energy storage systems, controllable loads, and electric vehicle charging stations, and are typically interfaced to the distribution system through inverters. Active Distribution Networks (ADNs) are MIMO-coupled systems due to the interaction among DERs. Adequate control of reactive power injections by DERs' inverters can provide significant support for the voltage regulation of the ADNs.

In this paper, the classical hierarchical decomposition of the voltage control problem is assumed [1]. At the primary control level, a local approach is adopted in which each DER unit is equipped with a PI-based voltage control unit that, based on local measures of the voltage amplitude of the network node at which the DER is connected, which adjusts the reactive power output of the inverter to impose the optimal voltage setpoint. The secondary control level calculates the setpoint values, determining an optimal voltage profile along the

distribution feeders, improving power quality, reducing active power losses, and increasing line security margins [2]. During the time evolution of the ADN operating conditions between two subsequent optimization problems, the reference reactive current output by the voltage PI regulator may exceed the reactive power capability constraint of the inverter. In this case, the DER control unit saturates, and the windup phenomenon occurs. In this circumstance, restoring the normal (unsaturated) mode in time is necessary to provide the reactive power imposed by the reference current, which nullifies the steady-state voltage regulation error.

Different control strategies have been devised in the literature to avoid the windup phenomenon. Generally, most design techniques have been developed for SISO plants and have progressively been extended to MIMO systems. The main anti-windup techniques range from adaptive [3–5], optimal [6,7], LMI-based [8–11], sliding mode control [12–15], to model predictive control [16–22] compensation method [23], and H_∞ control [24,25]. Although these techniques are widely available, the design algorithms still require intense mathematical manipulations due to nonlinearity. Moreover, anti-windup schemes for MIMO systems require intensive real-time data exchange among the local controllers. On the other hand, SISO anti-windup techniques, such as back-calculation and conditional integration [23,26,27], are simple to implement but may present unsatisfactory performance due to the neglected interaction of MIMO systems and chattering.

To avoid complex design and real-time communication, the present paper proposes a cooperative strategy among local DER control units, which is implemented by a distributed algorithm, namely the Distributed Cooperative Algorithm (DCA). If a DER control unit suffers saturation, all other DERs act as individual agents that utilize the communication infrastructure to share information and participate in solving the saturation. In detail, in the presence of saturation, the algorithm starts in each DER control unit, receiving the voltage errors from all other DERs and determining the voltage control loop's local optimal voltage setpoint variation. This variation is evaluated by assigning a share of the voltage error of the saturated DER unit to each DER according to a weighted average principle, where the averaging weights account for each DER's different impacts on the saturated unit's voltage error. The new setpoints pursue two objectives. The first results in a new value of the reference reactive current in each voltage control loop that avoids windup in the saturated DER unit. The second is to reduce the distance of the new voltage profile of all nodes where a DER is connected compared to the optimal one determined by the secondary control level. The algorithm operates with at a sampling rate of 1–2 s, much longer than the sampling time of the local control units and communication links. So, it can be safely assumed that the associated delays are zero and the communication requirements are limited, unlike the MIMO anti-windup control techniques that require real-time intensive information exchange among the control units of the DERs and communication infrastructures. The algorithm's convergence is guaranteed in the cases of multiple saturated DERs and of reduced communication among DERs. The latter occurs when the communication link connecting two DERs is unavailable.

In summary, the characteristics of the proposed DCA are listed below.

1. It uses fixed average weights and requires only the communication of the steady-state voltage errors among the control units of the DERs;
2. It is independent of the adopted design for voltage control. It is then possible to adopt low complexity controllers, such as PIs;
3. Its action reduces the distance of the actual voltage profile from the optimal one;
4. It presents a low computational burden; see Section 4 and limited communication requirements since the sample rate of the communication is of the order of seconds;
5. The transmission delays can be neglected;

6. It handles saturation of multiple DERs, regardless of the sign of voltage errors;
7. In the presence of limited communication among DERs, the DCA still reaches convergence, although its performance is affected; see Scenarios 3 and 4 in Section 5.

To give evidence of our contribution, a comparison between the proposed DCA and the main control strategies presented in the literature is reported in Table 1.

Table 1. Comparison with related control strategies presented in the literature.

Underlying Methodology and Reference	Information Exchanged with Neighbord	Type of Controller	Rate of Information Exchange	Anti-Windup Controller Design	Architecture	Impact of Communication Failure	Observers
Adaptive [3]	local state, auxiliary variables	nonlinear	high	yes	distributed	not verified	yes
Adaptive [4]	–	nonlinear	high	yes	centralized	not verified	no
Primal-dual optimizer [6]	multiplier, set-point	nonlinear	high	yes	distributed	not verified	no
Primal-dual optimizer [7]	physical quantities, auxiliary variables	nonlinear	high	yes	distributed	verified	no
LMI-based [8]	–	nonlinear	high	yes	centralized	not verified	no
LMI-based [9]	–	MIMO	high	yes	centralized	not verified	no
Sliding-mode control [13]	status of generators	nonlinear	high	yes	distributed	verified	no
MPC [16]	full state	nonlinear	high	yes	distributed	not verified	yes
MPC [20]	state and control	nonlinear	high	yes	distributed	not verified	no
Compensation [23]	–	linear	–	yes	decentralized	–	no
H_∞ control [25]	state and output	nonlinear	high	no	distributed	not verified	no
Proposed	local error	SISO	low	no	distributed	not verified	no

The remainder of this paper is organized as follows. Section 2 presents the ADN model in steady-state conditions. Section 3 illustrates the proposed cooperative strategy to avoid the windup. Section 4 discusses how the DCA works based on the previously described cooperative strategy. Section 5 reports the results of the numerical simulations developed for the IEEE 13-bus test feeder, and, finally, Section 6 draws conclusions and future research directions.

2. System Model

To model the steady-state operation of an Active Distribution Network (ADN), the DistFlow equations are typically employed, taking advantage of the grid's radial configuration [28]. Unfortunately, such equations are nonlinear. A typical simplified model linearizes the DistFlow equations into the LinDistFlow equations, which are derived by neglecting active and reactive power losses. From the LinDistFlow equations, a graph-based matrix representation is obtained, as detailed in [29], that can be partitioned by considering only the N nodes where DERs are connected, yielding

$$\Delta \boldsymbol{V} = \boldsymbol{V} - \boldsymbol{V}^0 = \boldsymbol{\Gamma}\ \boldsymbol{Q} \tag{1}$$

being $\boldsymbol{V}$ and $\boldsymbol{Q}$ the $(N \times 1)$ vectors of, respectively, DERs' nodal voltages and reactive power injections; $\boldsymbol{V}^0$ represents the value of $\boldsymbol{V}$ for $\boldsymbol{Q} = \boldsymbol{0}$ and $\boldsymbol{\Gamma}$ is the $(N \times N)$ matrix of sensitivity coefficients. In detail, the generic element γ_{ij} of $\boldsymbol{\Gamma}$ represents the sensitivity of the nodal voltage of ith DER to the injection of reactive power from jth DER. In [29], it is shown that $\boldsymbol{\Gamma}$ is symmetric and positive definite; moreover it is $\gamma_{ii} \geq \gamma_{ij} > 0$ for all i and j by construction.

Each DER is equipped with a PI-based voltage control unit that regulates the voltage at the connection node of the ADN to an assigned setpoint. The voltage regulation is obtained by acting on the reactive power injected by the DER through the inverter, which interfaces the DER to the grid. For this paper, the dynamic response of the DER voltage regulation is of no interest, and only steady-state behavior is considered. The control unit guarantees that the following vector of steady-state voltage errors

$$\boldsymbol{\epsilon} \triangleq \boldsymbol{V}^{sp} - \boldsymbol{V} \tag{2}$$

is null, where $\boldsymbol{V}^{sp}$ the $(N \times 1)$ is the vector of voltage setpoints. Usually, the value of $\boldsymbol{V}^{sp}$ is provided by the network optimization task at the secondary control level to guarantee adequate voltage profiles along the distribution feeders [1]. In the remainder, the vector of optimal setpoints is indicated as $\boldsymbol{V}^{sp,opt}$ and the steady-state voltage regulation error referred to $\boldsymbol{V}^{sp,opt}$ as

$$\bar{\boldsymbol{\epsilon}} \triangleq \boldsymbol{V}^{sp,opt} - \boldsymbol{V} \tag{3}$$

3. Cooperative Strategy

In the absence of saturation, it has $\boldsymbol{V}^{sp} = \boldsymbol{V}^{sp,opt}$ and, consequently, $\boldsymbol{\epsilon} = \bar{\boldsymbol{\epsilon}} = \boldsymbol{0}$. However, due to the voltage variations caused by, for example, changes in loads, active powers injected by DER, and supplying substation operating conditions, the reactive power output of the DER inverter may exceed its maximum given by the capability chart. In such circumstances, the reactive current of the inverter reaches its limit, the control unit saturates, and a non-zero steady-state error appears.

To avoid the windup, the proposed cooperative strategy introduces a variation of the setpoints as follows:

$$\boldsymbol{V}^{sp} = \boldsymbol{V}^{sp,opt} + \Delta\boldsymbol{V}^{sp} \tag{4}$$

asking also the unsaturated DERs to participate in solving the saturation. The aim is double: to solve the saturation of all DERs, obtaining a null value of $\boldsymbol{\epsilon}$ defined by (2); to reduce the distance of the overall voltage profile from the optimal one, that is, reducing the error $\bar{\boldsymbol{\epsilon}}$ defined by (3). It is worth noticing that changing the setpoint causes that $\boldsymbol{\epsilon} \neq \bar{\boldsymbol{\epsilon}}$.

Let us assume that the jth DER suffers saturation and, consequently, a steady-state regulation error $\bar{\epsilon}_j = V_j^{sp,opt} - V_j$ arises. Variations $\Delta\boldsymbol{V}^{sp}$ are evaluated by assigning a share of error $\bar{\epsilon}_j$ to each DER according to a weighted average principle, where the averaging weights account for the different impact of each DER on $\bar{\epsilon}_j$. This impact is quantified by the elements of the $(N \times 1)$ vector $\boldsymbol{\gamma}_j$ representing the transposed jth row of $\boldsymbol{\Gamma}$ or, equivalently, the jth column of $\boldsymbol{\Gamma}^T$. Then, normalizing the elements of $\boldsymbol{\gamma}_j$, the vector of the weights $\boldsymbol{w}$ is derived as

$$\boldsymbol{w} = \frac{1}{\| \boldsymbol{\gamma}_j \|_1} \boldsymbol{\gamma}_j \tag{5}$$

where $\| \boldsymbol{\gamma}_j \|_1$ is the 1-norm of $\boldsymbol{\gamma}_j$. The normalization (5) guarantees a unitary sum of the elements of $\boldsymbol{w}$, that is, $\| \boldsymbol{w} \|_1 = 1$.

Using the elements w_i of $\boldsymbol{w}$ as weights, the variations of the setpoints for all the unsaturated DERs can be derived as

$$\Delta V_i^{sp} = w_i \, \bar{\epsilon}_j \quad \text{for } i \neq j \tag{6}$$

whereas for the jth DER the variation ΔV_j^{sp} is composed of two terms

$$\Delta V_j^{sp} = -\bar{\epsilon}_j + w_j \bar{\epsilon}_j = -(1 - w_j)\,\bar{\epsilon}_j \tag{7}$$

to guarantee that $\sum_{i=1}^{N} \Delta V_i^{sp} = 0$.

The cooperative strategy represented by (5)–(7) can easily be extended to the general case in which multiple DERs suffer reactive power saturation.

Normalizing the elements of $\mathbf{\Gamma}^T$ by column, the matrix of the weights is derived as

$$\mathbf{A} = \mathbf{\Gamma}^T \mathbf{B} \tag{8}$$

where

$$\mathbf{B} = \text{diag}\left\{1/|\gamma_1|_1, 1/|\gamma_2|_1, \ldots, 1/|\gamma_N|_1\right\} \tag{9}$$

is the diagonal matrix whose jth diagonal element is the reciprocal of $\left|\gamma_j\right|_1$. It is trivial to verify that the jth column of $\mathbf{A}$ is equal to the vector of the weights $\boldsymbol{w}$ in (5). The normalization (8) guarantees that the columns of matrix $\mathbf{A}$ have unitary sum, that is, $\sum_{i=1}^{N} a_{ij} = 1, \forall\, j = 1, \ldots, N$. Moreover, from (8) and (9) and from the properties of the elements of $\mathbf{\Gamma}$, it is derived that $1 > a_{jj} \geq a_{ji} > 0$ for all i and j.

Then, (6) and (7) is cast in matrix form as

$$\Delta \boldsymbol{V}^{sp} = -\mathbf{L}\,\bar{\boldsymbol{\epsilon}} \tag{10}$$

with

$$\mathbf{L} = \mathbf{I} - \mathbf{A} \tag{11}$$

being $\mathbf{I}$ the $N \times N$ identity matrix.

In Appendix A, it is demonstrated that the eigenvalues of matrix $\mathbf{A}$ are all real and positive, being the largest eigenvalue $\lambda_A^{max} = 1$ with unitary multiplicity.

Concerning matrix $\mathbf{L} = \mathbf{I} - \mathbf{A}$, let $\boldsymbol{y}_i$ be the right-eigenvector of $\mathbf{A}$ corresponding to the eigenvalue λ_{Ai}; it results

$$\mathbf{L}\boldsymbol{y}_i = (\mathbf{I} - \mathbf{A})\boldsymbol{y}_i = \boldsymbol{y}_i - \mathbf{A}\boldsymbol{y}_i = \boldsymbol{y}_i - \lambda_{Ai}\,\boldsymbol{y}_i = (1 - \lambda_{Ai})\,\boldsymbol{y}_i \tag{12}$$

Then, $\boldsymbol{y}_i$ is also the right-eigenvector of $\mathbf{L}$ corresponding to the eigenvalue $\lambda_{Li} = 1 - \lambda_{Ai}$. From (12) and the properties of the eigenvalues of $\mathbf{A}$—see (A3)—it is trivial to derive that

$$0 = \lambda_L^{min} < (1 - \lambda_{A(N-1)}) \leq \ldots \leq (1 - \lambda_{A1}) < 1 \tag{13}$$

Consequently, $\mathbf{L}$ is a *Laplacian* matrix with $N - 1$ real eigenvalues, positive and smaller than a unit, and a null eigenvalue $\lambda_L^{min} = 0$ with unitary multiplicity, corresponding to the eigenvector $\bar{\mathbf{1}}$. The smallest non null eigenvalue $1 - \lambda_{A(N-1)}$ is the Laplacian *algebraic connectivity*.

Finally, it can be shown that applying (10) reduces the distance of the voltage profile from the optimal one concerning its starting value. The distance can be measured by the Euclidean norm $||\boldsymbol{V}^{sp,opt} - \boldsymbol{V}||_2$. Then, the starting distance is the norm $||\bar{\boldsymbol{\epsilon}}||_2$ of the steady-state regulation error; see (3). Applying (10) the distance becomes; see (4)

$$||\Delta \boldsymbol{V}^{sp}||_2 = ||\mathbf{L}\,\bar{\boldsymbol{\epsilon}}||_2$$

The distance is reduced because it stands

$$||\mathbf{L}\,\bar{\boldsymbol{\epsilon}}||_2 < ||\bar{\boldsymbol{\epsilon}}||_2 \tag{14}$$

In Appendix B, the proof of inequality (14) is reported assuming $N = 2$ for the sake of readability.

4. Proposed DCA

An iterative algorithm implementing the cooperative strategy (10) is derived to update in real time the value of the setpoint vector $\boldsymbol{V}^{sp}$. At the kth iteration step, first the local voltage control unit of each DER evaluates its element of $\boldsymbol{\epsilon}(k)$, that is, the vector of steady-state voltage errors defined as; see (2):

$$\boldsymbol{\epsilon}(k) = \boldsymbol{V}^{sp}(k-1) \; - \; \boldsymbol{V}(k) \tag{15}$$

In (15), $\boldsymbol{V}^{sp}(k-1)$ is the vector of setpoints evaluated by the algorithm and sent to the control units at the previous iteration step. $\boldsymbol{V}(k)$ is the vector of actual steady-state values of the measured voltages. Then, the vector of the voltage setpoints is updated according to the rule

$$\boldsymbol{V}^{sp}(k) = \boldsymbol{V}^{sp}(k-1) \; - \; \mathbf{L}\,\boldsymbol{\epsilon}(k) \tag{16}$$

Since $\mathbf{L}$ is a Laplacian matrix, from the graph theory [30], it can be stated that there exists an average equilibrium which is reached by the iterative algorithm (16). The convergence is not typically reached with only one iteration for three reasons: i. the choice of the weights does not impose a null error with only one iteration step, ii. the model (1) is approximated, and iii. the variations of the voltage setpoints may cause some DERs previously operating in linearity to suffer saturation in the following steps. The Laplacian algebraic connectivity is a measure of the speed of convergence of the iterative algorithm [30].

Each element of $\boldsymbol{\epsilon}(k)$ is available at the local control unit of each DER, which can send its voltage regulation error to all other control units and can receive, in turn, the errors evaluated by all control units. Then, once the local image of the vector $\boldsymbol{\epsilon}(k)$ has been built, the distributed implementation of the iterative algorithm (16) is straightforward. The jth DER stores the elements of the jth row of $\mathbf{L}$ and, at each iteration step, locally evaluates its new setpoint $V_j^{sp}(k)$, according to (16). The block diagram of the DCA in the frame of the two-level architecture for voltage control is sketched in Figure 1.

In general, it is possible to remove the assumption of one-to-one data exchange among all the DERs. Let us assume that the ith DER does not exchange the voltage regulation error with the jth DER. Then, the elements γ_{ij} and γ_{ji} of matrix $\boldsymbol{\Gamma}$ in (1) are set to zero. All the developments concerning the cooperative strategy are still valid. The matrix $\mathbf{L}$ remains a Laplacian matrix with the same properties, provided that connectivity of the graph is guaranteed, that is, there is a communication path connecting the ith to the jth DER through other DERs. The convergence of the iterative algorithm is also guaranteed, but the speed is decreased because the Laplacian algebraic connectivity is reduced.

The practical implementation of the DCA according to Figure 1 requires that its time step be large enough to ensure the voltage control loop's transient response decay. Moreover, it must be compatible with the communication channel characteristics among the DERs. At the same time, it must be small enough to guarantee that it can promptly account for the changes in the operating conditions between two subsequent optimizations of the second control level. A time step on the order of one to a few seconds is considered appropriate; see Figure 1. Moreover, a persistence interval can be implemented to prevent premature algorithm activation. In practice, each DER waits for a predetermined number of consecutive time steps during which saturation is sustained before transmitting a non-zero error signal to the other DERs. Finally, when at the time step h—see Figure 1—the secondary control level evaluates and sends to the DERs the new optimal values of the setpoints, the DCA is reset by imposing $\boldsymbol{V}^{sp}(0) = \boldsymbol{V}^{sp,opt}(h)$.

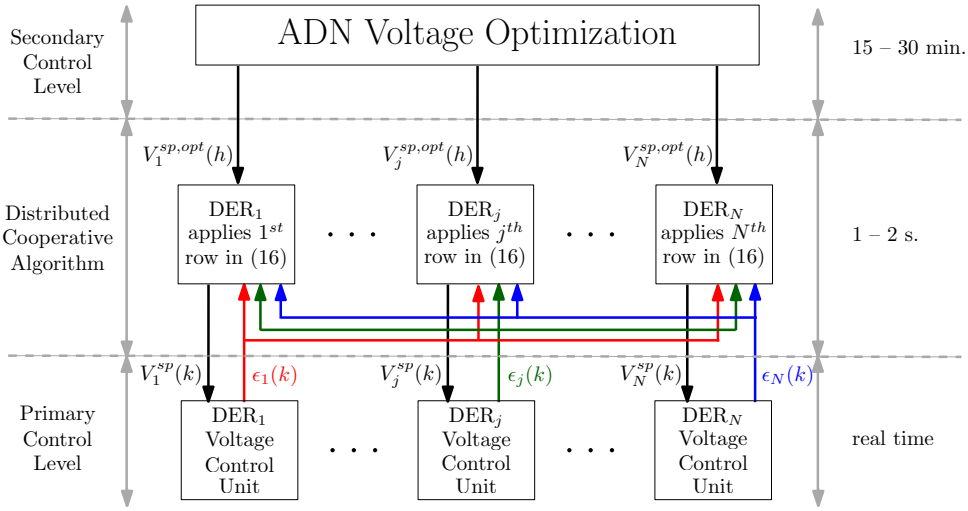

Figure 1. Block diagram of the distributed cooperative algorithm in the frame of the two-level architecture for voltage control.

The steps to implement the DCA are briefly summarized in the following, referring to the basic example of the simple feeder shown in Figure 2.

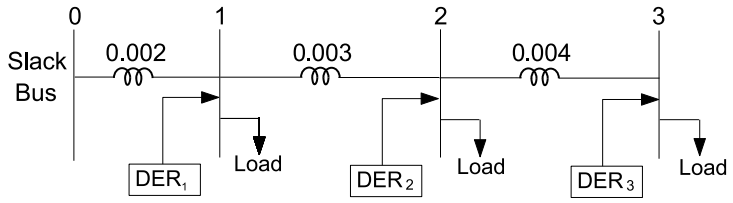

Figure 2. Simple feeder for the basic example.

The offline steps consist of evaluating the following in order:

- The sensitivity matrix $\mathbf{\Gamma}$ in (1) by feeder inspection;
- Matrix $\mathbf{A}$ using (8);
- Matrix $\mathbf{L}$ using (11).

In the basic example in Figure 2, the results are

$$\mathbf{\Gamma} = \begin{bmatrix} 0.002 & 0.002 & 0.002 \\ 0.002 & 0.005 & 0.005 \\ 0.002 & 0.005 & 0.009 \end{bmatrix} \quad \mathbf{A} = \begin{bmatrix} 2/6 & 2/12 & 2/16 \\ 2/6 & 5/12 & 5/16 \\ 2/6 & 5/12 & 9/16 \end{bmatrix} \quad \mathbf{L} = \begin{bmatrix} 4/6 & -2/12 & -2/16 \\ -2/6 & 7/12 & -5/16 \\ -2/6 & -5/12 & 7/16 \end{bmatrix} \tag{17}$$

Then, each DER is provided for the corresponding row of matrix $\mathbf{L}$.

Concerning the steps of the online implementation, let the generic k^{th} iteration be considered assuming that all the DER control units are in linear unsaturated operation with the following steady-state conditions

$$\boldsymbol{V}(k) = \boldsymbol{V}^{sp}(k) = \boldsymbol{V}^{sp,opt} = [1 \quad 1 \quad 1]^T \tag{18}$$

then, both $\bar{\boldsymbol{\epsilon}}(k) = \boldsymbol{V}^{sp,opt} - \boldsymbol{V}(k)$ and $\boldsymbol{\epsilon}(k) = \boldsymbol{V}^{sp}(k) - \boldsymbol{V}(k)$ are null.

Let the operating conditions of the ADN vary, causing voltage variations and the reaction of the DER voltage control loops. Let DER$_2$ reach positive saturation so that its control unit keeps a steady-state voltage regulation error equal to 0.01. Then, at the next $(k+1)$th iteration step of the DCA it stands

$$\boldsymbol{V}(k+1) = [1 \quad 0.99 \quad 1]^T$$

The DCA iteration step is performed with the following two steps:

- The DER control units exchange their voltage errors yielding the local image of the error vector $\boldsymbol{\epsilon}(k+1) = [0 \quad 0.01 \quad 0]^T$;
- Each DER control unit corrects its voltage setpoint using its row of matrix $\mathbf{L}$ according to (16), obtaining

$$\boldsymbol{V}^{sp}(k+1) = \boldsymbol{V}^{sp}(k) \; - \; \mathbf{L}\,\boldsymbol{\epsilon}(k+1) = \; [1+0.02/12 \quad 1-0.07/12 \quad 1+0.05/12]^T$$

The DER voltage control loops will try to impose the new setpoint values. Let us assume that in the subsequent transient, both DER_1 and DER_3 remain in linear unsaturated operation, so that they reach a null steady-state voltage regulation error. If the DER_2 control unit desaturates, then $\boldsymbol{\epsilon}$ becomes zero and the DCA has reached its objective. On the contrary, if the DER_2 control unit remains in saturation, then its reactive power does not change. Assuming that the model (1) represents the actual response of the ADN, the steady-state operating conditions that are reached by the DER control units are obtained by imposing the following conditions:

$$\Delta V_1 = 0.02/12, \quad \Delta V_3 = 0.05/12, \quad \Delta Q_2 = 0$$

to the ADN linear model $\Delta \boldsymbol{V} = \boldsymbol{\Gamma}\, \Delta \boldsymbol{Q}$, where the voltage variations are evaluated with respect to $\boldsymbol{V}(k+1)$. The solution of the three linear equations of the ADN model yields

$$\Delta Q_1 = 5/8, \quad \Delta Q_3 = 5/24, \quad \Delta V_2 = 0.055/24$$

Consequently, at the next $(k+2)$th iteration step of the DCA, it stands

$$\begin{aligned} \boldsymbol{V}(k+2) &= [1+0.02/12 \quad 0.99+0.055/24 \quad 1+0.05/12]^T \\ \boldsymbol{\epsilon}(k+2) &= \boldsymbol{V}^{sp}(k+1) - \boldsymbol{V}(k+2) = [0 \quad 0.045/24 \quad 0]^T \\ \bar{\boldsymbol{\epsilon}}(k+2) &= \boldsymbol{V}^{sp,opt} - \boldsymbol{V}(k+2) = [0.02/12 \quad 0.185/24 \quad 0.05/12]^T \end{aligned}$$

The improvement of the distance of the voltage amplitudes from the optimal setpoint values is quantified by evaluating the Euclidean norm of $\bar{\boldsymbol{\epsilon}}$ yielding

$$\| \; \bar{\boldsymbol{\epsilon}}(k+2) \; \|_2 = 0.00892 \; < \; 0.01 = \| \; \bar{\boldsymbol{\epsilon}}(k+1) \; \|_2$$

Concerning the voltage regulation errors, it is apparent that $\boldsymbol{\epsilon}_2(k+2) = 0.001875$ is one order of magnitude smaller than $\boldsymbol{\epsilon}_2(k+1) = 0.01$. Continuing the iteration of the above computations yields the time evolution of the voltage regulation error of DER_2 shown in Figure 3, giving evidence that the DCA tends to converge.

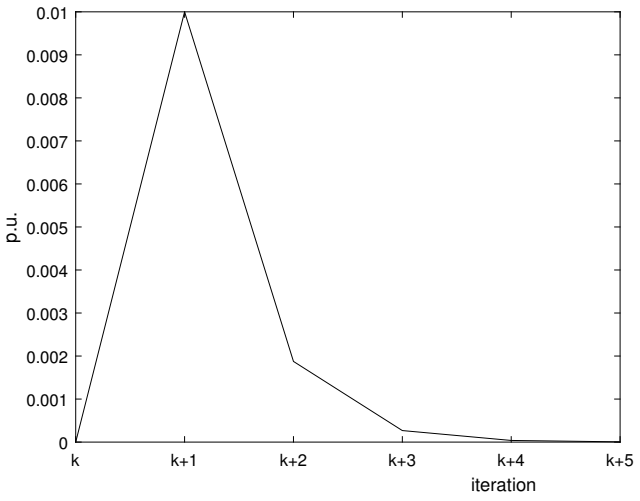

Figure 3. Evolution of the voltage regulation error $\boldsymbol{\epsilon}_2$ of DER_2 for the basic example.

5. Numerical Simulations

The schematic diagram of the simulated ADN is shown in Figure 4. It is obtained by duplicating the IEEE 13-bus Test Feeder [31], and balancing both lines and loads. Therefore, the capacity of the HV/MV transformer is doubled and set to 10 MVA. Three distributed energy resources (DERs) are connected to each feeder. Each DER is capable of injecting up to 600 kW of active power and can modulate its reactive power within approximately ±300 kVAr (the actual value depends on the operating conditions of the network node and the configuration of the filter at the point of common coupling (PCC)). The full network load equals about 3 MW of active power and 2 MVAr of reactive power. All simulations were performed using PSCAD/EMTDC® 4.5 for the ADN, the PV systems, and the local voltage control unit, and MATLAB® R2010b for the DCA. The adopted solution time step is 50 µs, with a relative convergence tolerance of 10^{-5}. The local PI control units were designed according to the methodology presented in [32] and used across all the simulations. The reactive power saturation is locally managed by a classical SISO anti-windup technique included in PSCAD/EMTDC® PI model. In particular, the conditional integration scheme, also known as the integrator clamping scheme, is adopted. Referring to the jth DER, according to Figure 5, when the voltage control unit enters saturation, the input to the integrator is forced to zero.

The results of two case studies are presented and discussed in the following. *Case study A: Load connection*. *Case study B: Load disconnection*. In both cases, the following four different scenarios were analyzed, which differ only in the features of the DCA.

Scenario 1: The DCA is absent; consequently, when a DER control unit suffers saturation and the steady-state voltage regulation error is not null, no variation is imposed on the setpoints of either the saturated DER or the other DERs.

Scenario 2: All six DERs exchange the local steady-state voltage error and, consequently, vary their setpoints. The resulting Lagrangian matrix is

$$\mathbf{L} = \begin{bmatrix} 0.6407 & -0.2306 & -0.2847 & -0.0834 & -0.0778 & -0.0720 \\ -0.1704 & 0.7239 & -0.1757 & -0.0834 & -0.0778 & -0.0720 \\ -0.2761 & -0.2306 & 0.6608 & -0.0834 & -0.0778 & -0.0720 \\ -0.0647 & -0.0876 & -0.0668 & 0.7349 & -0.2048 & -0.2287 \\ -0.0647 & -0.0876 & -0.0668 & -0.2196 & 0.6431 & -0.1895 \\ -0.0647 & -0.0876 & -0.0668 & -0.2651 & -0.2048 & 0.6342 \end{bmatrix} \tag{19}$$

Scenario 3: DERs connected to the same feeder exchange the voltage errors, whereas, between the two feeders, only DER_3 and DER_4 exchange data. The resulting Lagrangian matrix is

$$\mathbf{L} = \begin{bmatrix} 0.5541 & -0.3127 & -0.3286 & 0.0 & 0.0 & 0.0 \\ -0.2115 & 0.6255 & -0.2028 & 0.0 & 0.0 & 0.0 \\ -0.3426 & -0.3127 & 0.6085 & -0.1001 & 0.0 & 0.0 \\ 0.0 & 0.0 & -0.0770 & 0.6819 & -0.2672 & -0.2917 \\ 0.0 & 0.0 & 0.0 & -0.2636 & 0.5344 & -0.2417 \\ 0.0 & 0.0 & 0.0 & -0.3181 & -0.2672 & 0.5334 \end{bmatrix} \tag{20}$$

Scenario 4: Some data exchanges among DERs connected to the same feeder are missing. Moreover, the communication between the DERs of the two different feeders is absent. The Lagrangian matrix is not fully connected, resulting in the following:

$$\mathbf{L} = \begin{bmatrix} 0.5541 & -0.4551 & -0.4563 & 0.0 & 0.0 & 0.0 \\ -0.2115 & 0.4551 & 0.0 & 0.0 & 0.0 & 0.0 \\ -0.3426 & 0.0 & 0.4563 & 0.0 & 0.0 & 0.0 \\ 0.0 & 0.0 & 0.0 & 0.6465 & -0.3647 & -0.3847 \\ 0.0 & 0.0 & 0.0 & -0.2929 & 0.3647 & 0.0 \\ 0.0 & 0.0 & 0.0 & -0.3535 & 0.0 & 0.3847 \end{bmatrix} \quad (21)$$

The DCA is implemented with a time step of 1 s and a persistence interval of 2 s for all Scenarios 2, 3, and 4, which differ only in the communication structure of the DCA.

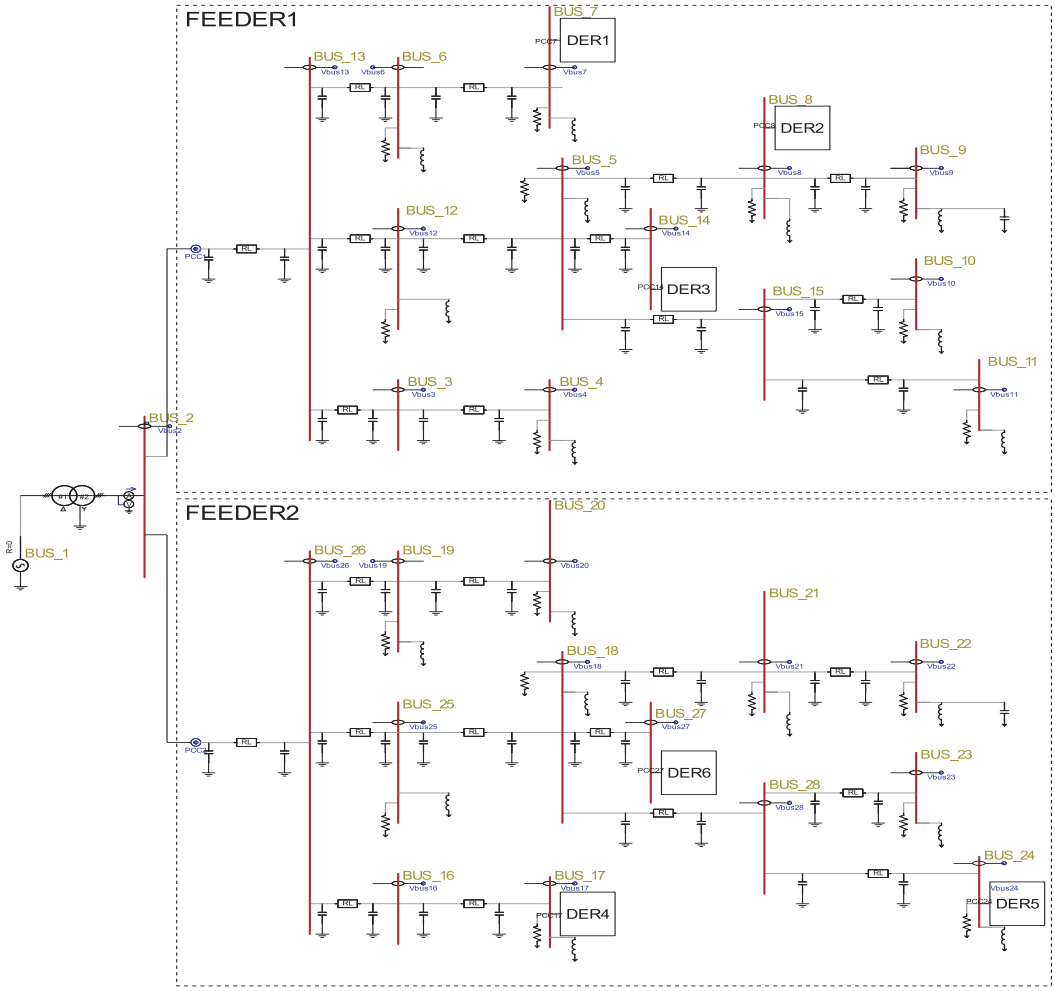

Figure 4. PSCAD representation of the considered ADN composed of two IEEE test feeders.

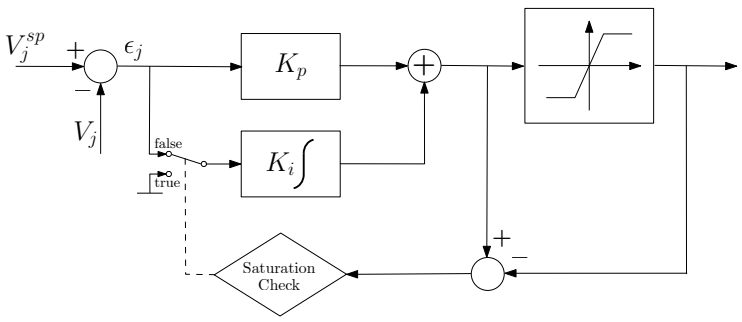

Figure 5. Local anti-windup scheme for the PI control unit of the jth DER.

5.1. Case Study A—LOAD Connection

The network is assumed to supply half of the full network load. The active power injection of DERs is equal to 300 kW, and the slack bus voltage is set to 1.03 p.u.

The vector of the optimal setpoint is set equal to

$$\boldsymbol{V}^{sp,opt} = [1.02,\ 1.00,\ 1.03,\ 1.00,\ 1.00,\ 1.00]^T$$

Starting from steady-state operating conditions, at time $t = 15$ s, a load (0.5 MW–0.5 MVAr) is connected to bus 23 of the second feeder (first perturbation). Subsequently, at time $t = 20$ s, an additional load (about 0.42 MW–0.23 MVAr) is connected to bus 9 of the first feeder (second perturbation).

5.1.1. Case Study A—Scenario 1—Local Classical Anti-Windup Technique (No DCA)

The time evolution of voltages and setpoints for the DERs is depicted in Figure 6, evidencing the voltage perturbations introduced by the load connections at time instants $t = 15$ s and $t = 20$ s. The time evolution of the reactive powers injected by the DERs according to the action of the voltage control units in response to the two perturbations is reported in Figure 7.

It is worth noticing that in this case and in all the rest of the cases, the reactive power injected into the grid includes the reactive power injected by the inverter, which is subject to current saturation limits, and the reactive power injected by the filter, which is connected between the inverter and the grid.

From these figures, it is apparent that, after the response of the local voltage control units to the first voltage perturbation caused by load connection along feeder 2, DER_5 suffers reactive power saturation, and its voltage does not reach the optimal setpoint at steady-state. Since each control unit acts by itself, no other units help to reduce the saturation effects. The setpoint is not varied according to the local anti-windup scheme in Figure 5. Since the DCA is absent, no further action is present, and there are no further transient variations of either voltage or reactive power injections for all the DERs after the transient response to the voltage perturbation.

Similar considerations can be made concerning the time evolution after the second load connection at time instant $t = 20$ s. In this case, DER_3 suffers reactive power saturation after the transient response, and its voltage does not reach the optimal setpoint at steady-state. Also, in this case, the setpoint is not varied, and a non-null voltage error also appears for DER_3, which is exactly on its saturation limit.

In conclusion, it can be stated that in this case, in the presence of saturation, non-null voltage errors result.

To quantify the effect of saturation on the voltage profile, the values of the difference between the optimal setpoints and the actual steady-state nodal voltages are reported in Table 2. In particular, the first row refers to the steady-state operation after the first perturbation, whereas the second row refers to the steady-state operation after the second perturbation. The last column reports the values of the Euclidean norm representing the overall distance of the actual voltage profile from the optimal one. From this table, the following is apparent:

- After the first perturbation, DER_5 is the only DER presenting a non-null difference due to saturation, and the Euclidean norm is equal to such a value;
- After the second perturbation, DER_3 also presents a non-null difference due to saturation, and the difference for DER_5 is slightly increased; the Euclidean norm accounts for both these non-null values.

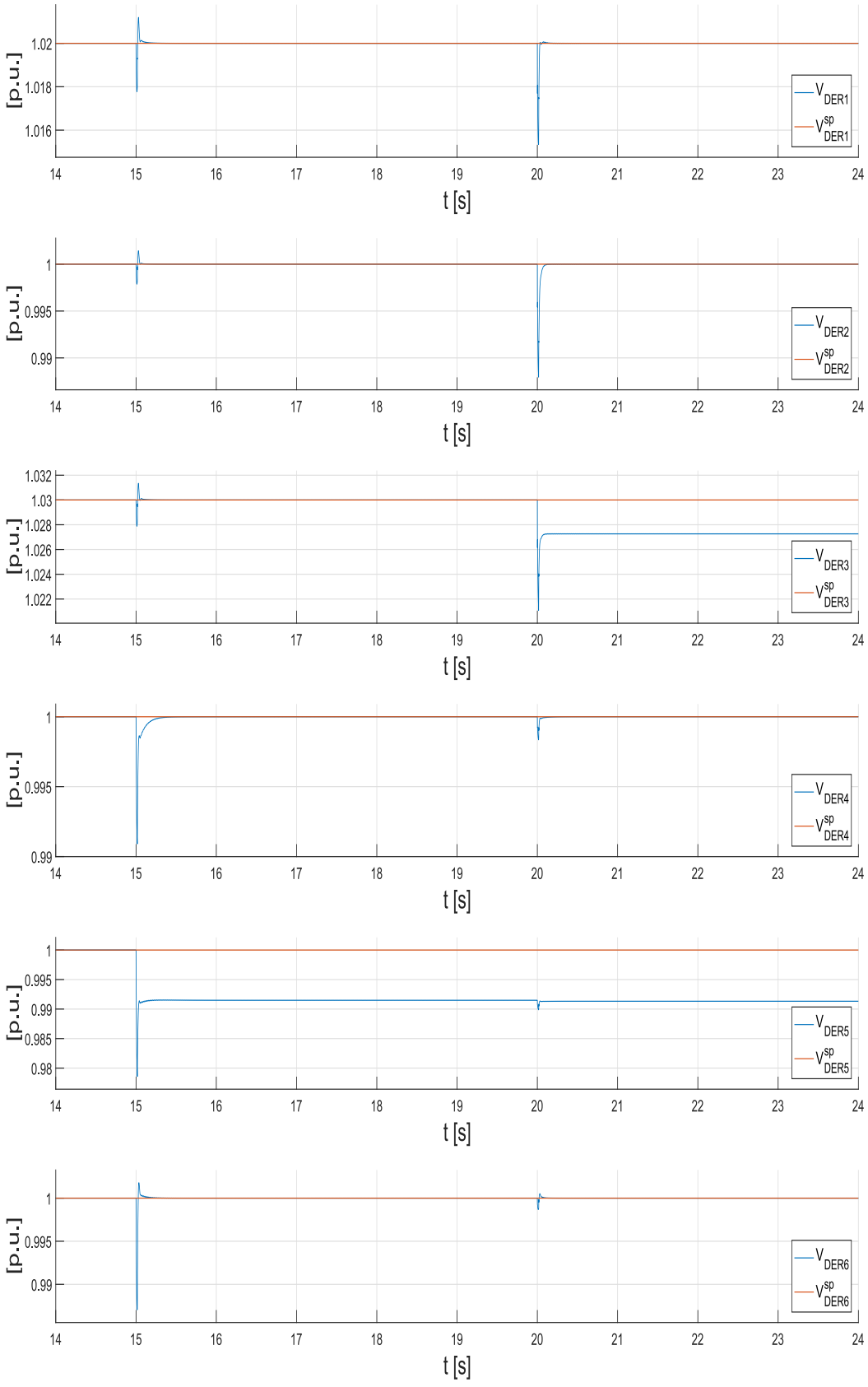

Figure 6. Case study A—Scenario 1: Time evolution of voltages and setpoints for each DER.

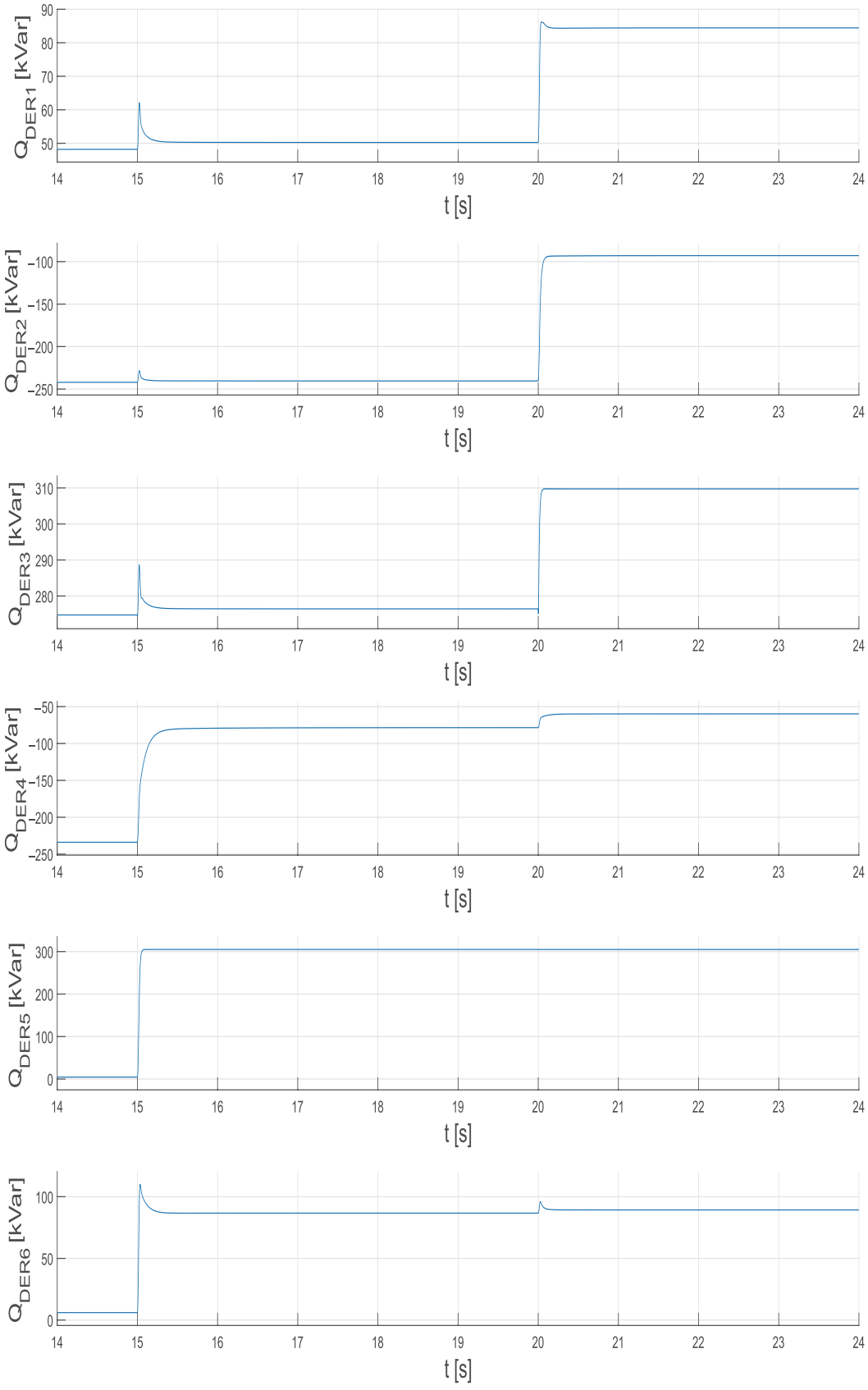

Figure 7. Case study A—Scenario 1: Time evolution of reactive power injections by each DER.

Table 2. Case study A—Scenario 1: Difference between optimal setpoints and nodal voltages.

Perturbation	$V^{sp,opt} - V$ **(10^{-3} p.u.)**						$\| V^{sp,opt} - V \|_2$ **(10^{-3} p.u.)**
	DER_1	DER_2	DER_3	DER_4	DER_5	DER_6	
after 1	0.00	0.00	0.00	0.00	8.51	0.00	8.51
after 2	0.00	0.00	2.74	0.00	8.67	0.00	9.09

5.1.2. Case Study A—Scenario 2—DCA with Full Data Exchange Among DERs

The time evolution of voltages and setpoints and of the reactive power injections for all the DERs are reported in Figures 8 and 9, respectively. Immediately after the two perturbations due to load connections at time instants $t = 15$ s and $t = 20$ s, they present the same voltage control loop responses as the ones in Scenario 1. The different behavior appears after the persistence interval of 2 s, that is, at $t = 17$ s, when the DCA varies the setpoints of all the DERs according to matrix $\mathbf{L}$ in (19). From the figures, it is apparent that the second group of three DERs that are connected to the second feeder provides the largest contribution to counteract the saturation of DER_5. It is related to the values of the coefficients of the 5th column of the matrix (19), which are derived from the sensitivity matrix $\mathbf{\Gamma}$ of the physical model (1). Indeed, the reactive power injections of the DERs connected to the first feeder have a small impact on the voltages of the second feeder, because they affect only the voltage drop on the substation transformer. Similar considerations can be made for the second perturbation that concerns a load connection along feeder 1, causing saturation of DER_3, and the action of the DCA affecting mainly the first three DERs that are connected to the same feeder 1. Finally, from Figure 8, it is evident that after both the saturation events, the DCA reaches convergence in two to three steps of iteration.

For the sake of comparison with Scenario 1, the results in terms of the difference and the distance between the optimal and the actual voltage profiles are reported in Table 3. In particular, the first and the second row refer to the values reached at convergence of the DCA, respectively, after the first and the second perturbation. Analyzing the values in Table 3, the following can be observed:

- The DCA with full data exchange involves all the DERs introducing a non-null value of the difference for all the DERs; in particular, the DERs that do not suffer saturation present a negative voltage difference because they cooperate to reduce the positive voltage difference in the saturated DERs;
- After the first perturbation, the largest contribution (represented by the largest absolute value of the negative voltage differences) is provided by DER_4 and DER_6 that are connected to the same feeder as DER_5, which suffers saturation;
- After the second perturbation, the largest changes in the voltage variations with respect to the variations in the first row concern DER_1 and DER_2, which are connected to the same feeder as DER_3, which suffers saturation.

Comparing the results in Table 3 with the corresponding ones in Table 2, it is apparent that after both saturation events, the action of the DCA reduces the distance of the actual voltage profile from the optimal one with respect to the local anti-windup classical techniques. Numerically, from the last column, it is apparent that the DCA reduces the Euclidean norm of the distance by about 9%.

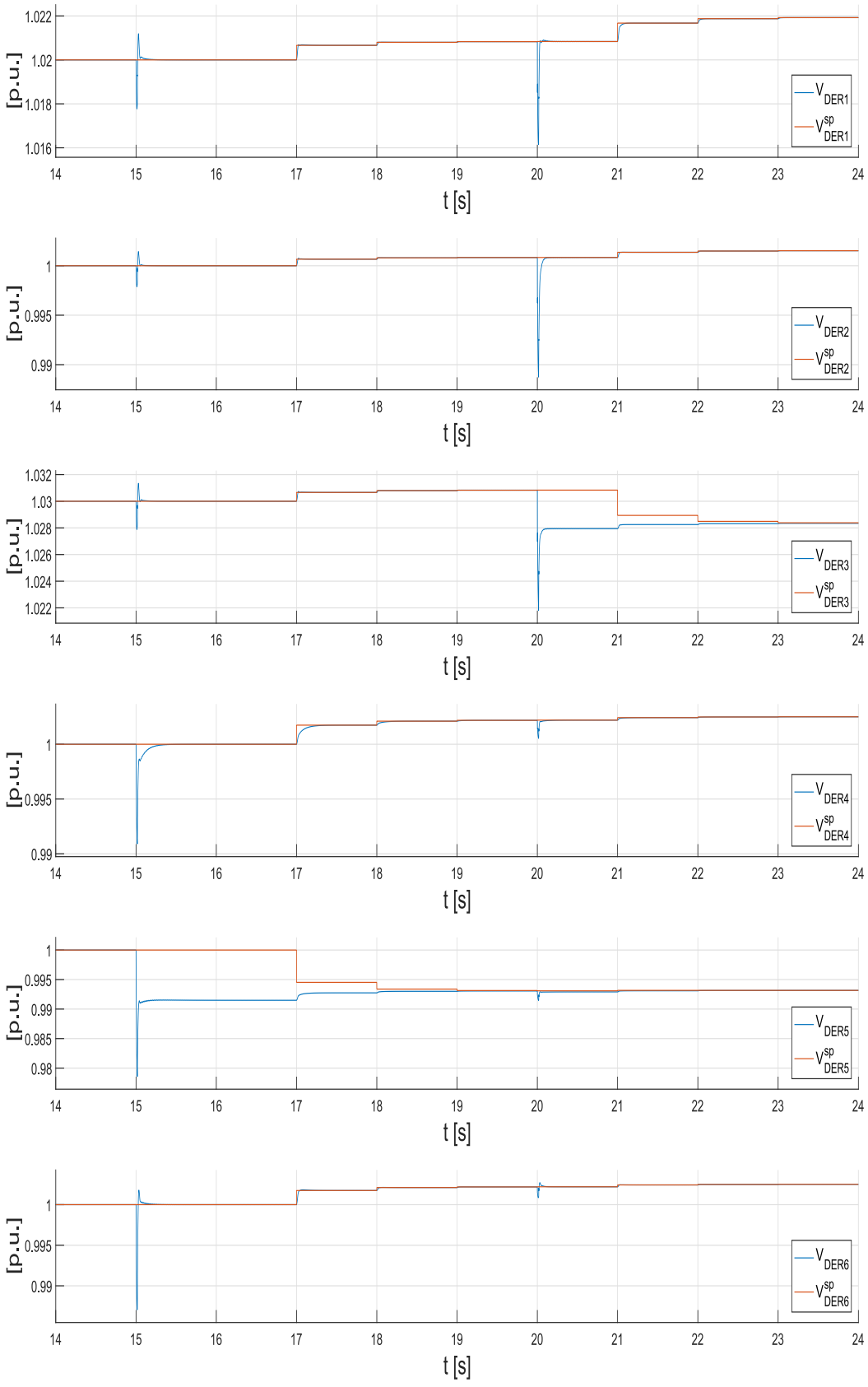

Figure 8. Case study A—Scenario 2: Time evolution of voltages and setpoints for each DER.

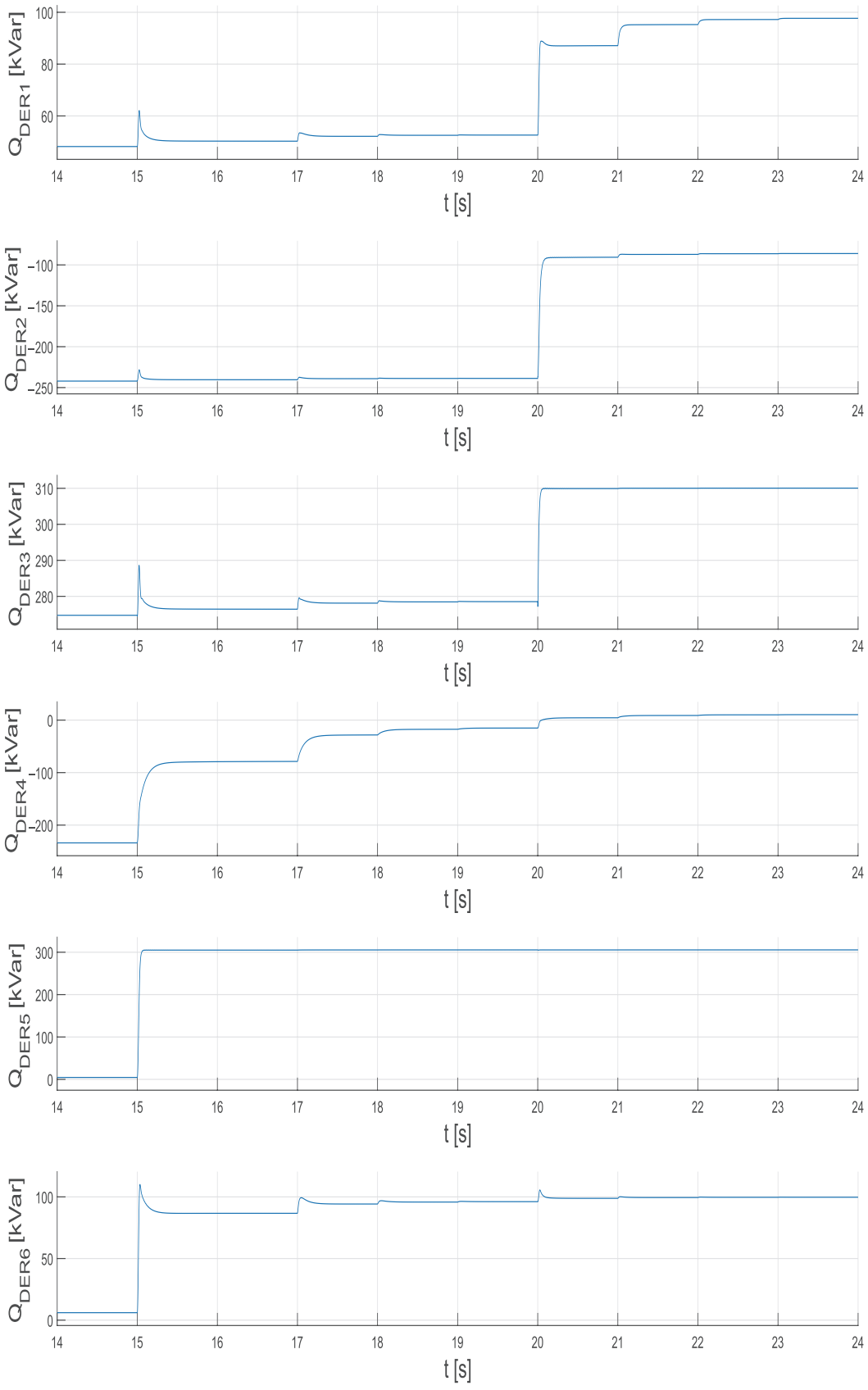

Figure 9. Case study A—Scenario 2: Time evolution of reactive power injections by each DER.

Table 3. Case study A—Scenario 2: Difference between optimal setpoints and nodal voltages.

Perturbation	$V^{sp,opt} - V$ (10^{-3} **p.u.**)						$\| V^{sp,opt} - V \|_2$ (10^{-3} **p.u.**)
	DER_1	DER_2	DER_3	DER_4	DER_5	DER_6	
after 1st	−0.83	−0.83	−0.83	−2.18	6.94	−2.18	7.73
after 2nd	−1.94	−1.52	1.65	−2.51	6.84	−2.51	8.26

5.1.3. Case Study A—Scenario 3—DCA with Limited Data Exchange Between the DERs of Different Feeders

Concerning the transients of voltages and reactive power injections, the dynamics do not significantly differ from Scenario 2, so the related graphs are omitted for brevity. Attention is focused only on the different steady-state operating conditions that are obtained due to the setpoint changes imposed by DCA in the case of saturation. It is important to report that the algorithm reaches convergence in this scenario in three steps.

Similarly to the other scenarios, the steady-state results in terms of the difference and the distance between the optimal and the actual voltage profiles are reported in Table 4. In particular, the first and the second row refer to the values reached at convergence of the DCA, respectively, after the first and the second perturbation.

After the first perturbation, the DCA changes to setpoints of the second group of three DERs connected to the second feeder to counteract the saturation of DER_5. In contrast, the DCA does not act on the DERs connected to the first feeder. It is due to the zero values of the coefficients of the fifth column of the matrix (20) that cause no action of the DERs of the first feeder in response to the saturation of DER_5. Similar considerations can be made for the second perturbation that concerns a load connection along the first feeder, causing saturation of DER_3. The DCA action mainly affects the first three DERs connected to the same feeder, and marginally DER_4. The very small variations of DER_5 and DER_6 are induced by the action of the other DERs. Analyzing the values in Table 4, the following can be stated:

- The DCA with partial data exchange can involve only part of the DERs, introducing negligible values of the difference for some of them; for example, see the zeros for the DERs of the first feeder after the first perturbation that causes saturation of DER_5 on the second feeder;
- After the first perturbation, the larger voltage variations concern the DER_4 and DER_6 that are connected to the same feeder as DER_5, which suffers saturation;
- After the second perturbation that brings DER_3 into saturation, the larger increase in the absolute value of the voltage variations concerns the DER_1, according to the elements of the third column of matrix (20).

Comparing the last column in Table 4 with the corresponding one in Table 2 for Scenario 1, it is apparent that the action of the DCA reduces the distance of the actual voltage profile from the optimal one, after both saturation events. Numerically, the Euclidean norm of the distance is reduced by about 10%, which is even slightly better than Scenario 2. The reason is related to the small effect that the reactive power injections of the DERs of one feeder have on the voltages of the other feeder, and consequently, reducing the communication among the DERs of the different feeders does not have a significant impact on the performance of the DCA in terms of voltage profile enhancement.

Table 4. Case study A—Scenario 3: Difference between optimal setpoints and nodal voltages.

Perturbation	$V^{sp,opt} - V$ **(10^{-3} p.u.)**						$\| V^{sp,opt} - V \|_2$ **(10^{-3} p.u.)**
	DER_1	DER_2	DER_3	DER_4	DER_5	DER_6	
after 1st	0.00	0.00	0.00	−3.08	6.34	−3.08	7.69
after 2nd	−1.04	−0.64	1.92	−3.39	6.30	−3.15	8.14

5.1.4. Case Study A—Scenario 4—DCA with Limited Data Exchange Between the DERs of the Same Feeder and No Data Exchange Among the DERs of Different Feeders

For the same reasons as in Scenario 3, the graphs with the time evolution of voltages and reactive powers are omitted for brevity. The algorithm reaches convergence in this scenario in three to four steps; as expected, the convergence is slowed down due to the presence of several zero elements in matrix (21).

Similarly to the other scenarios, the results in terms of the difference and the distance between the optimal and the actual voltage profiles are reported in Table 5. In particular, the first and the second row refer to the values reached at convergence of the DCA, respectively, after the first and the second perturbation.

After the first perturbation, DER_5 is brought into saturation, and the DCA changes the setpoints of DER_5 and DER_4 to counteract the saturation effects. As for Scenario 3, the DERs connected to the first feeder do not contribute, and, in addition, also DER_6 is not involved. It is due to the corresponding zero element in the fifth column of matrix (21). Similar considerations can be made for the second perturbation that causes saturation of DER_3. Such saturation is counteracted by the action on the only DER_1; see the zero elements of the third column of matrix (21). The variations of the voltages on the second feeder caused by DCA action on DER_1 cause the DCA action with some small setpoint corrections also for the DER_5 and DER_4 of the second feeder.

Analyzing the values in Table 5, the following can be observed:

- The DCA with very limited data exchange can involve only a few of the DERs;
- After the first perturbation, causing saturation of DER_5, the only voltage variations concern the DER_4 and DER_5 itself;
- After the second perturbation, causing saturation of DER_3, the only significant voltage variations concern the DER_1 and DER_3 itself.

Table 5. Case study A—Scenario 4: Difference between optimal setpoints and nodal voltages.

Perturbation	$V^{sp,opt} - V$ **(10^{-3} p.u.)**						$\| V^{sp,opt} - V \|_2$ **(10^{-3} p.u.)**
	DER_1	DER_2	DER_3	DER_4	DER_5	DER_6	
after 1st	0.00	0.00	0.00	−5.20	6.04	0.00	7.97
after 2nd	−1.76	0.00	1.77	−5.85	5.85	0.00	8.64

Comparing the last column in Table 5 with the corresponding one in Table 2, it is apparent that the action of the DCA still reduces the distance of the actual voltage profile from the optimal one, after both saturation events. However, the Euclidean norm of the distance is reduced by about 5–6%, which is less than Scenarios 3 and 4.

5.2. Case Study B—Load Disconnection

The network is assumed to supply half of the full network load. The active power injection of DERs is equal to 300 kW, and the slack bus voltage is set to 1.03 pu.

The vector of the optimal setpoint is set equal to

$$\boldsymbol{V}^{sp,opt} = [1.03,\ 0.985,\ 1.02,\ 1.00,\ 0.98,\ 1.00]^T$$

The starting steady-state operating conditions include the presence of two additional loads, namely the first load (0.5 MW–0.5 MVAr) at bus 23 of the second feeder and the second load (0.42 MW–0.23 MVAr) at bus 9 of the first feeder. At time $t = 15$ s, the first load is disconnected (first perturbation) and then, at time $t = 20$ s, the second load is also disconnected (second perturbation).

5.2.1. Case Study B—Scenario 1—Local Classical Anti-Windup Technique (No DCA)

The time evolution of voltages and setpoints for the DERs is depicted in Figure 10, evidencing the two voltage perturbations introduced by the load disconnections at time instants, respectively, $t = 15$ s and $t = 20$ s. The time evolution of the reactive powers injected by the DERs according to the action of the voltage control units in response to the two perturbations is reported in Figure 11. From these figures, it is apparent that, after the response of the local voltage control units to the first voltage perturbation caused by load connection along the second feeder, DER_5 suffers reactive power saturation, reaching its minimum value around -300 kVAr. Consequently, its voltage does not reach the optimal setpoint at steady state. Since each control unit acts by itself, no other units help to reduce the saturation's effects. The setpoint is not varied according to the local anti-windup scheme in Figure 5. Since the DCA is absent, no further action is present, and there are no subsequent variations of either voltage or reactive power injections for all the DERs, which simply adapt themselves to the new equilibrium state. Since the DCA is absent, no further action is present, and there are no further transient variations of either voltage or reactive power injections for all the DERs after the transient response to the voltage perturbation.

Similar considerations can be made concerning the time evolution after the second load disconnection at time instant $t = 20$ s. In this case, DER_2 suffers reactive power saturation, reaching its lower limit of about -300 kVAr after the transient response, and its voltage does not reach the optimal setpoint at steady-state. Also, in this case, the setpoint is not varied, and a non-null voltage error also appears for DER_2, which is exactly on its saturation limit.

In conclusion, it can be stated that in this case, in the presence of saturation, non-null voltage errors result.

To quantify the effect of saturation on the voltage profile, the values of the difference between the optimal setpoints and the actual steady-state nodal voltages are reported in Table 6. In particular, the first row refers to the steady-state operation after the first perturbation, whereas the second row refers to the steady-state operation after the second perturbation. The last column reports the values of the Euclidean norm representing the overall distance of the actual voltage profile from the optimal one. From this table, it is apparent that

- After the first perturbation, DER_5 is the only DER presenting a non-null difference due to saturation, and the Euclidean norm is equal to such a value;
- After the second perturbation, also DER_2 presents a non-null difference due to saturation, and the difference for DER_5 is slightly increased; the Euclidean norm accounts for both these non-null values.

Table 6. Case study B—Scenario 1: Difference between optimal setpoints and nodal voltages.

Perturbation	$V^{sp,opt} - V$ (10^{-3} **p.u.**)						$\| V^{sp,opt} - V \|_2$ (10^{-3} **p.u.**)
	DER_1	DER_2	DER_3	DER_4	DER_5	DER_6	
after 1st	0.00	0.00	0.00	0.00	−11.91	0.00	11.91
after 2nd	0.00	−8.15	0.00	0.00	−12.14	0.00	14.63

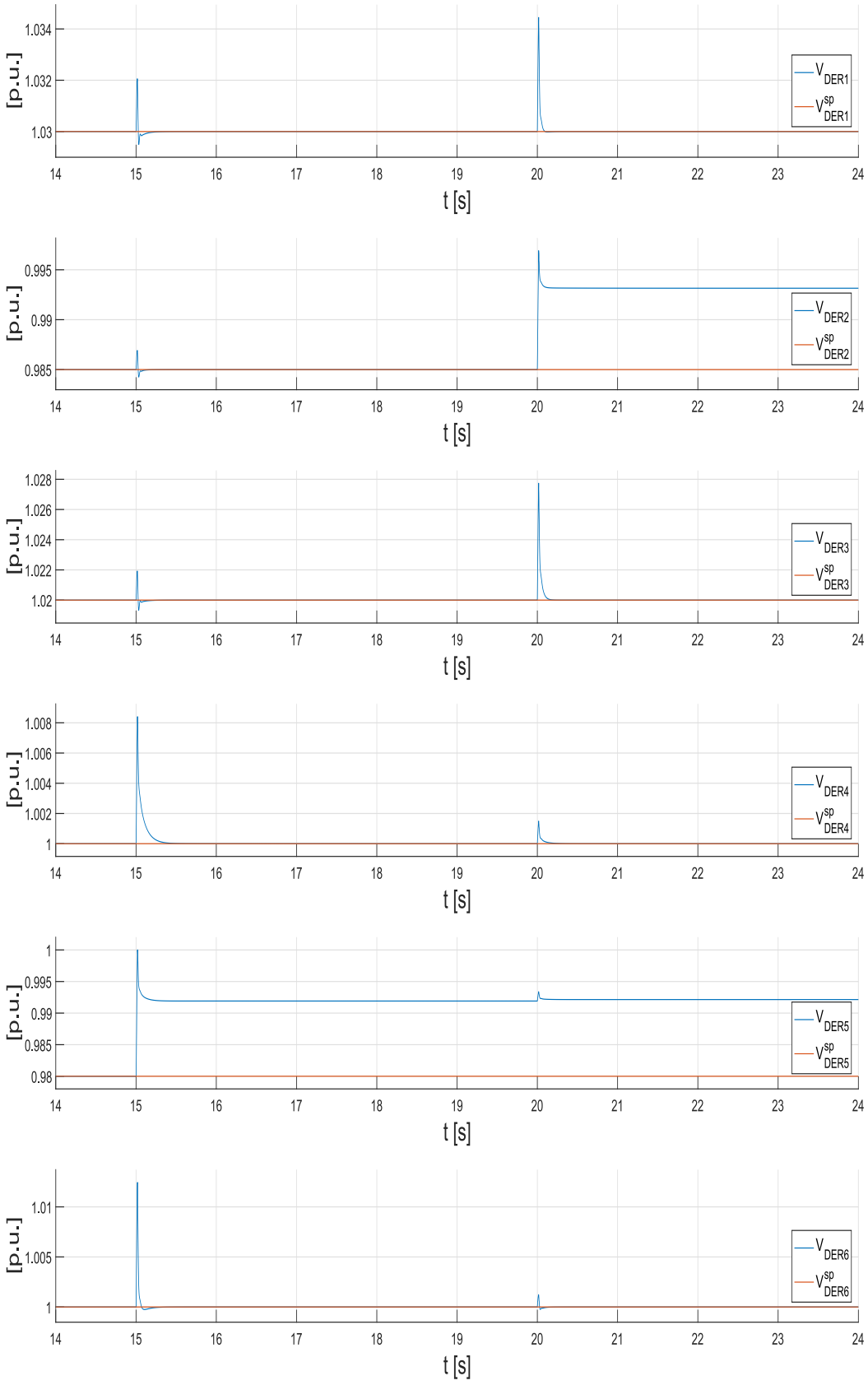

Figure 10. Case study B—Scenario 1: Time evolution of voltages and setpoints for each DER.

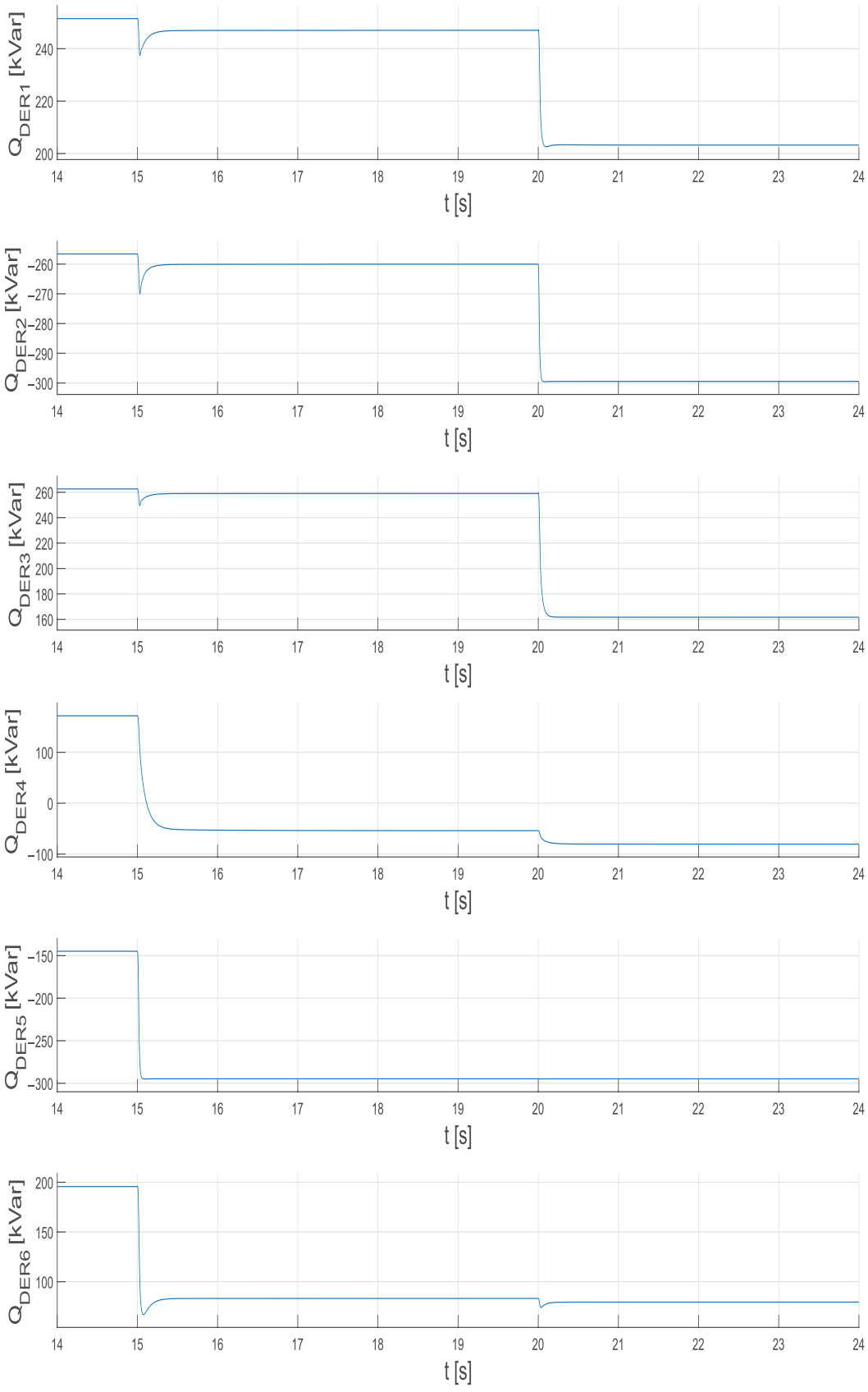

Figure 11. Case study B—Scenario 1: Time evolution of reactive power injections by each DER.

5.2.2. Case Study B—Scenario 2—DCA with Full Data Exchange Among DERs

The time evolution of voltages and setpoints and of the reactive power injections for all the DERs are reported in Figures 12 and 13, respectively. They present the same voltage perturbations and voltage control loop responses to the load disconnection at time instants $t = 15$ s and $t = 20$ s as the ones in Scenario 1. The different behavior appears after the persistence interval of 2 s, that is, at $t = 17$ s, when the DCA varies the setpoints of all the DERs according to matrix **L** in (19). From the figures, it is apparent that the second group of three DERs that are connected to the second feeder provides the largest contribution to counteract the saturation of DER_5. It is related to the values of the coefficients of the 5th column of the matrix (19). Similar considerations can be made for the second perturbation that concerns a load disconnection along the first feeder, causing saturation of DER_2, and the action of the DCA affecting mainly the first three DERs that are connected to the same feeder. Finally, from Figure 12, it is evident that after both the saturation events, the DCA converges in two to three steps.

Similarly to Scenario 1, the results in terms of the difference and the distance between the optimal and the actual voltage profiles are reported in Table 7. In particular, the first and the second row refer to the values reached at convergence of the DCA, respectively, after the first and the second perturbation. Analyzing the values in Table 7, the following can be observed:

- The DCA with full data exchange involves all the DERs introducing a non-null value of the difference for all the DERs; in particular, the DERs that do not suffer saturation present a positive voltage difference because they cooperate to reduce the negative voltage difference in the saturated DERs;
- After the first perturbation, the largest contribution (represented by the largest value of the positive voltage differences) is provided by DER_4 and DER_6 that are connected to the same feeder as DER_5, which suffers saturation;
- After the second perturbation, the largest changes in the voltage variations with respect to the variations in the first row concern DER_1 and DER_2 that are connected to the same feeder as DER_3, which suffers saturation.

Comparing the last column in Table 7 with the corresponding one in Table 6, it is apparent that the DCA action reduces the distance of the actual voltage profile from the optimal one, after both saturation events. Numerically, the DCA reduces the Euclidean norm of the distance by 9%.

Table 7. Case study B—Scenario 2: Difference between optimal setpoints and nodal voltages.

Perturbation	$\boldsymbol{V^{sp,opt} - V}$ **(10^{-3} p.u.)**						$\boldsymbol{\| V^{sp,opt} - V \|_2}$ **(10^{-3} p.u.)**
	DER_1	DER_2	DER_3	DER_4	DER_5	DER_6	
after 1st	1.16	1.16	1.16	3.05	−9.67	3.05	10.78
after 2nd	3.51	−6.02	3.51	4.05	−9.10	4.05	13.29

5.2.3. Case Study B—Scenario 3—DCA with Limited Data Exchange Between the DERs of Different Feeders

For the same reasons as in Case study A—Scenario 3, the graphs with the time evolution of voltages and reactive powers are omitted for brevity. The algorithm reaches convergence in this scenario in three to four steps.

Similarly to the other scenarios, the steady-state results in terms of the difference and the distance between the optimal and the actual voltage profiles are reported in Table 4. In particular, the first and the second row refer to the values reached at convergence of the DCA, respectively, after the first and the second perturbation.

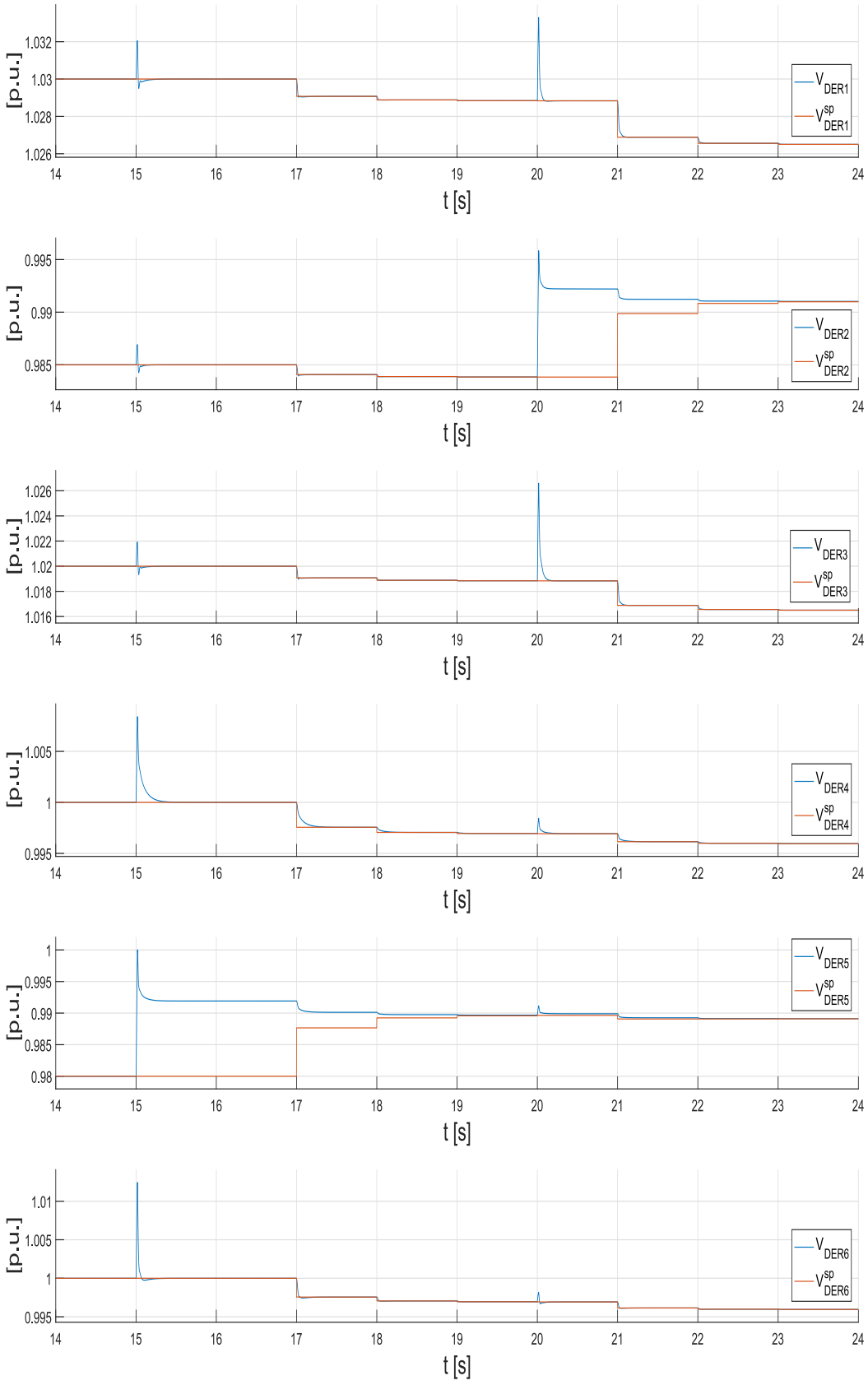

Figure 12. Case study B—Scenario 2: Time evolution of voltages and setpoints for each DER.

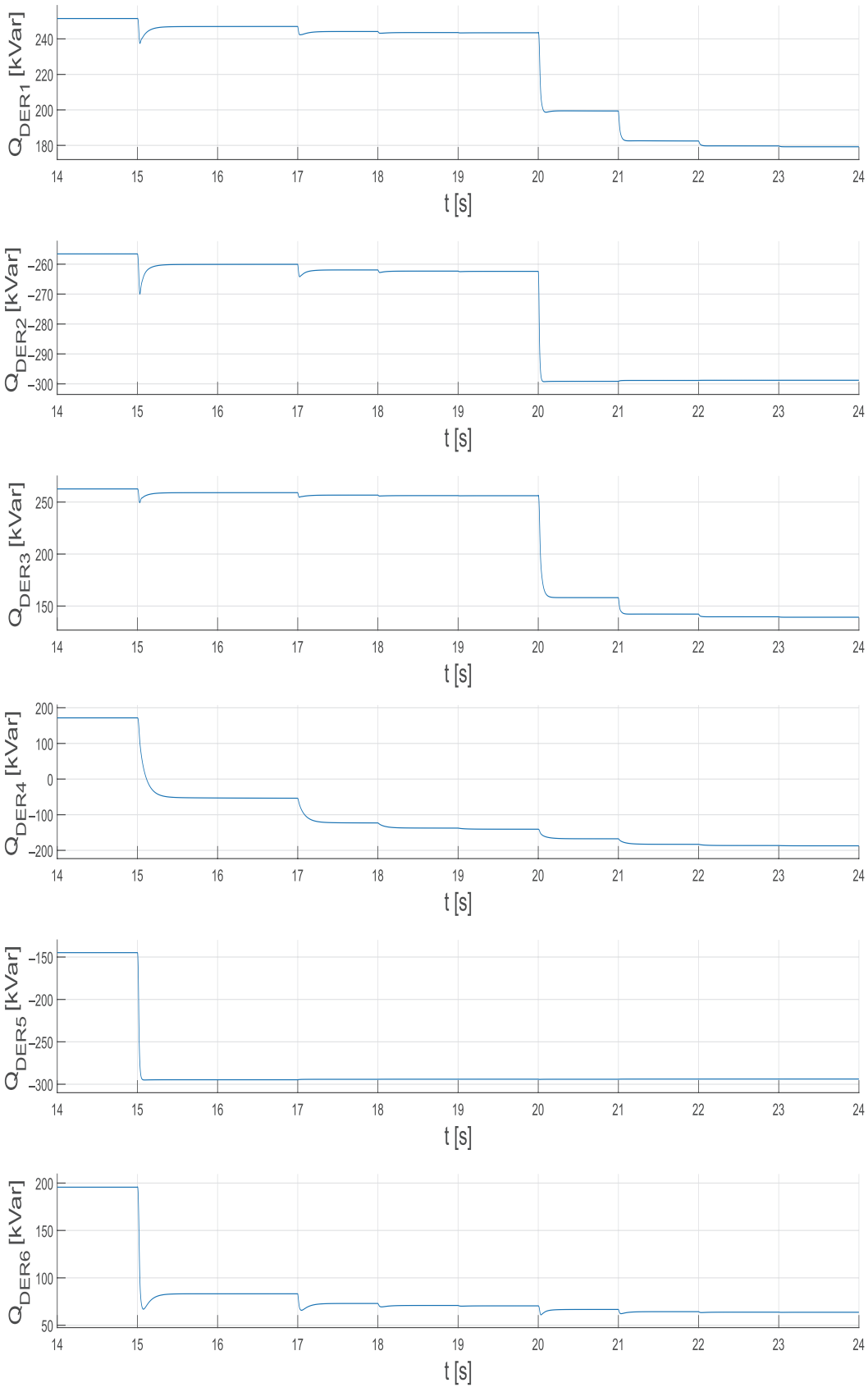

Figure 13. Case study B—Scenario 2: Time evolution of reactive power injections by each DER.

After the first perturbation, the DCA changes to setpoints of the second group of three DERs connected to the second feeder to counteract the saturation of DER_5. In contrast, the DCA does not act on the DERs connected to the first feeder. It is due to the zero values of the coefficients of the fifth column of the matrix (20) that cause no action of the DERs of the first feeder in response to the saturation of DER_5. Similar considerations can be made for the second perturbation that concerns a load disconnection along the first feeder, causing saturation of DER_2. The DCA action mainly affects the first three DERs connected to the same feeder, and marginally DER_4, DER_5, and DER_6. Analyzing the values in Table 8, similar conclusions can be drawn as the ones itemized in the previous Case study A—Scenario 3.

Table 8. Scenario 3—Difference between optimal setpoints and nodal voltages.

Perturbation	$V^{sp,opt} - V$ (10^{-3} p.u.)						$\| V^{sp,opt} - V \|_2$ (10^{-3} p.u.)
	DER_1	DER_2	DER_3	DER_4	DER_5	DER_6	
after 1st	0.00	0.00	0.00	4.29	−8.83	4.29	10.72
after 2nd	3.08	−6.16	3.08	4.43	−8.85	4.43	13.20

Comparing the last column in Table 8 with the corresponding one in Table 6, it is apparent that the action of the DCA reduces the distance of the actual voltage profile from the optimal one, after both saturation events. Numerically, the Euclidean norm of the distance is reduced by about 10%, which is even slightly better than Scenario 2. The conclusion is that reducing the communication among the DERs of the different feeders has no significant impact on the performance of the DCA in terms of voltage profile enhancement.

5.2.4. Case Study B—Scenario 4—DCA with Limited Data Exchange Between the DERs of the Same Feeder and No Data Exchange Among the DERs of Different Feeders

For the same consideration, as in Case study A—Scenario 3, the voltage and reactive power trends are omitted for brevity. Also, in this case, the algorithm continues to converge in three to four steps.

Similarly to the other scenarios, the results in terms of the difference and the distance between the optimal and the actual voltage profiles are reported in Table 9. In particular, the first and the second row refer to the values reached at convergence of the DCA, respectively, after the first and the second perturbation.

After the first perturbation, DER_5 is brought into saturation, and the DCA changes the setpoints of DER_5 and DER_4 to counteract the saturation effects. As for Scenario 3, the DERs connected to the first feeder do not contribute, and, in addition, DER_6 is also not involved. It is due to the corresponding zero element in the fifth column of matrix (21). The second perturbation causes saturation of DER_2. Such saturation is counteracted by the action on the only DER_1; see the zero elements of the third column of matrix (21). The variations of the voltages on the second feeder caused by DCA action on DER_1 cause the DCA action with some setpoint corrections also for the DER_5 and DER_4 of the second feeder. These latter corrections also cause the saturation of DER_4, which is counteracted by the DCA acting on the setpoint of DER_6, according to the non-null elements of the fourth column of matrix (21).

Analyzing the values in Table 9, similar conclusions can be drawn as the ones itemized in the previous Case study A—Scenario 4. The additional observation is that after the two perturbations, there are three DERs at their saturation limits, whereas in all the other scenarios, saturation concerns only two DERs.

Table 9. Scenario 4—Difference between optimal setpoints and nodal voltages.

Perturbation	$V^{sp,opt} - V$ (10^{-3} p.u.)						$\| V^{sp,opt} - V \|_2$ (10^{-3} p.u.)
	DER_1	DER_2	DER_3	DER_4	DER_5	DER_6	
after 1st	0.00	0.00	0.00	6.48	−8.78	0.00	10.91
after 2nd	6.40	−6.40	0.00	6.51	−8.46	1.76	14.10

Comparing the last column in Table 9 with the corresponding one in Table 6, it is apparent that the action of the DCA still reduces the distance of the actual voltage profile from the optimal one, after both saturation events. However, the Euclidean norm of the distance is reduced by about 8% after the first perturbation and 4% after the second perturbation, which is less than Scenarios 3 and 4. The worse performance after the second perturbation is related to the additional saturation of DER_4.

5.3. Discussion and Comparison Among the Scenarios

By comparing the results obtained in the considered scenarios, it can be stated that the DCA reaches convergence in a few steps, from two to four steps; the number of steps increases with the decrease in direct data exchange among DERs, according to the corresponding decrease in the Laplacian algebraic connectivity. Concerning the effectiveness of cooperation, it can be concluded that the DCA generally provides an improvement of the voltage profile with respect to Scenario 1. The distance from the optimal voltage profile is reduced by about 9% with Scenario 2, by about 10% with Scenario 3, and by about 4–8% with Scenario 4. From these results, it can be stated that the data exchange is relevant for the performance of the DCA, provided that it concerns DERs that are significantly coupled in the sensitivity matrix $\mathbf{\Gamma}$.

The considered scenarios present different steady-state values of the reactive power injections by the DERs because of the different cooperation among the DERs. To quantify this effect, Tables 10 and 11 report, respectively, for case studies A and B, the variations of the reactive power injection of each DER caused by the DCA action for Scenarios 2, 3, and 4, assuming as reference the corresponding value of the reactive power injection in Scenario 1. Moreover, the last columns of the tables report the overall reactive power variations, calculated as the sum of the absolute values of the six variations. From the analysis of Tables 10 and 11, it is evident that, when full exchange of the voltage errors takes place among all the DERs, i.e., Scenario 2, the variations of the reactive power injections of the DERs which do not suffer saturation present the same sign, i.e., they are all positive in case study A and all negative in case study B. This is not always true when some data exchange is missing and, consequently, some DERs present values with the discordant sign. Moreover, it is evident that DER_4, which presents the largest contribution in terms of reactive power variation, in Scenarios 3 and, even more, 4, is subject to larger variations. Finally, the values of the sum in the last column give further evidence that reducing the data exchange among the DERs, from Scenario 2 to Scenario 3 and, further, to Scenario 4, increases the overall reactive power variation. The above considerations are important because they imply that in Scenarios 3 and, especially, 4, the risk of further DERs suffering saturation after the DCA intervention is higher with respect to Scenario 2, which guarantees a better cooperation and sharing of the reactive power variation among the DERs. This is also testified for Scenario 4 by the fact that, after the second perturbation in case study B, there is an additional DER reaching saturation with respect to the other Scenarios.

Table 10. Case study A—Variation of reactive power with respect to Scenario 1.

Perturbation		**ΔQ (kVAr)**						**∑|ΔQ| (kVar)**
		DER_1	DER_2	DER_3	DER_4	DER_5	DER_6	
after 1st	Scenario 2	2.4	1.7	2.1	63.4	0.5	9.5	79.4
	Scenario 3	−6.6	−5.3	−5.4	95.3	0.7	14.1	127.4
	Scenario 4	−9.8	−7.8	−8.0	201.6	0.7	−39.2	267.2
after 2nd	Scenario 2	13.4	6.9	0.3	70.3	0.6	10.5	102.0
	Scenario 3	2.7	−2.7	0.2	103.3	0.7	12.1	121.7
	Scenario 4	8.4	−15.3	0.3	223.5	0.8	−44.8	293.1

Table 11. Case study B—Variation of reactive power with respect to Scenario 1.

Perturbation		**ΔQ (kVAr)**						**∑|ΔQ| (kVar)**
		DER_1	DER_2	DER_3	DER_4	DER_5	DER_6	
after 1st	Scenario 2	−3.6	−2.4	−2.9	−86.6	0.7	−12.7	108.9
	Scenario 3	9.3	7.2	7.5	−129.3	0.9	−19.0	173.3
	Scenario 4	12.3	9.6	9.9	−241.2	0.9	49.4	323.3
after 2nd	Scenario 2	−24.1	0.6	−22.5	−107.0	0.9	−15.9	171.0
	Scenario 3	−19.0	0.6	−17.7	−119.8	1.0	−17.7	175.8
	Scenario 4	−61.7	0.5	28.0	−214.8	1.1	30.3	336.4

6. Conclusions

In the frame of a two-level decomposition of the voltage control problem in ADN, the objective of avoiding a non-zero steady-state voltage error due to the windup of a voltage control unit caused by the saturation of the reactive power of DERs has been pursued. A cooperative strategy has been defined based on the idea of distributing the error among all control units, and a distributed cooperative algorithm has been derived. Each DER is equipped with the proposed DCA that, based on a share of the received errors, evaluates a variation of the voltage setpoint that desaturates all DERs and determines a voltage profile closer to the optimal one. The share of the errors is determined on the basis of average weights that account for the different impact of each DER on the saturated DERs. From the numerical simulations, it can be stated that the DCA always reaches convergence and improves the actual voltage profile, reducing its distance from the optimal setpoints. Concerning the cases of limited data exchange among the DERs, it has been proved that the missing communication between two DERs has a significant impact the performance of the DCA only if the electrical coupling between the two DERs is significant. Further research is investigating different approaches to define the weights to improve the performance of the DCA in terms of the reduction in the distance of the obtained voltage profile from the optimal one. The major drawback of the present formulation of the proposed DCA is that it requires some sort of synchronization of the communication among DERs. In fact, at the beginning of each iteration, DERs exchange their local voltage regulation errors to locally update their own voltage setpoints. Such a synchronization may practically not be viable; in addition, temporary failure of communication channels may impact on the synchronization. However, since matrix $\mathbf{L}$ is a Laplacian matrix, the results of the existing literature in the field of asynchronous average consensus algorithms can be extended to the proposed DCA. Then, future research will focus on choosing the best asynchronous strategy among the various ones proposed in the literature [33,34] to be applied to the DCA when synchronization is not guaranteed.

Author Contributions: Writing—original draft, G.M.C., G.F. and M.R.; conceptualization, G.F. and M.R.; methodology, G.F. and M.R.; software, G.M.C.; validation software, G.M.C.; writing—review and editing, G.M.C., G.F. and M.R.; funding acquisition, M.R. All authors have read and agreed to the published version of the manuscript.

Funding: This research was funded by Project ECS 0000024 "Ecosistema dell'innovazione—Rome Technopole" financed by EU in NextGenerationEU plan through MUR Decree n. 1051 23.06.2022 PNRR Mission 4 Component 2 Investment 1.5—CUP H33C22000420001.

Conflicts of Interest: The authors declare no conflict of interest.

Appendix A

In the remainder, it is shown that the eigenvalues of matrix $\mathbf{A}$ defined by (8) are all real and positive, and the largest eigenvalue is $\lambda_A^{max} = 1$ with unit multiplicity.

Let us begin by observing that matrix $\mathbf{A}$ has a unitary eigenvalue. Defining $\bar{\mathbf{1}}$, the row vector with all unit elements, from the property of the unitary sum of all columns of $\mathbf{A}$, it is trivial to verify that $\bar{\mathbf{1}}$ is the left-eigenvector associated with the unitary eigenvalue, that is,

$$\bar{\mathbf{1}}^T \mathbf{A} = \bar{\mathbf{1}}^T$$

The remaining $N-1$ eigenvalues are real and positive. Since $\mathbf{\Gamma}$ is invertible, $\mathbf{A}$ is also invertible and has no null eigenvalues. Moreover, suppose that $\boldsymbol{x}_i$ is the i-th left-eigenvector of the eigenvalue $\lambda_{A\,i} \neq 0$

$$\lambda_{A\,i}\, \boldsymbol{x}_i^T = \boldsymbol{x}_i^T \mathbf{A} = \boldsymbol{x}_i^T\, \mathbf{\Gamma}^T\, \mathbf{B}$$

Post-multiplying first by $\mathbf{B}^{-1}$

$$\lambda_{A\,i}\, \boldsymbol{x}_i^T\, \mathbf{B}^{-1} = \boldsymbol{x}_i^T\, \mathbf{\Gamma}^T \tag{A1}$$

and then by $\boldsymbol{x}_i$, it yields

$$\lambda_{A\,i} \left(\boldsymbol{x}_i^T\, \mathbf{B}^{-1}\, \boldsymbol{x}_i \right) = \boldsymbol{x}_i^T\, \mathbf{\Gamma}^T\, \boldsymbol{x}_i$$

Since $\mathbf{B}^{-1}$ and $\mathbf{\Gamma}^T$ are symmetric and positive definite, it follows that $\boldsymbol{x}_i^T\, \mathbf{B}^{-1}\, \boldsymbol{x}_i$ and $\boldsymbol{x}_i^T\, \mathbf{\Gamma}^T\, \boldsymbol{x}_i$ are real and positive. Hence, $\lambda_{A\,i}$ is also real and positive.

Since all elements of $\mathbf{A}$ are real and positive, according to the Perron–Frobenius theorem [35], $\lambda_A^{max} = 1$ has unitary multiplicity.

Now, consider the Equation (A1) written in term of 1-norm

$$\lambda_{A_i} \parallel \boldsymbol{x}_i^T\, \mathbf{B}^{-1} \parallel_1 = \parallel \left(\mathbf{\Gamma}\, \boldsymbol{x}_i \right)^T \parallel_1 = \parallel \mathbf{\Gamma}\, \boldsymbol{x}_i \parallel_1 \tag{A2}$$

Since $\mathbf{B}^{-1} = \mathrm{diag}\{\parallel \boldsymbol{\gamma}_j \parallel_1\}$, it has

$$\parallel \boldsymbol{x}_i^T\, \mathbf{B}^{-1} \parallel_1 = \sum_{i=1}^{N} \Big| \parallel \boldsymbol{\gamma}_i \parallel_1 \; x_i \Big| = \sum_{i=1}^{N} |x_i| \parallel \boldsymbol{\gamma_i} \parallel_1$$

Moreover,

$$\begin{aligned} \parallel \mathbf{\Gamma}\, \boldsymbol{x}_i \parallel_1 &= \sum_{j=1}^{N} \Big| (\mathbf{\Gamma}\, \boldsymbol{x}_i)_j \Big| = \sum_{j=1}^{N} \Big| \sum_{k=1}^{N} \gamma_{jk}\, x_k \Big| \leq \sum_{j=1}^{N} \sum_{k=1}^{N} |\gamma_{jk}\, x_k| = \sum_{j=1}^{N} \sum_{k=1}^{N} \gamma_{jk} |x_k| \\ &= \sum_{k=1}^{N} |x_k| \sum_{j=1}^{N} \gamma_{jk} = \sum_{k=1}^{N} |x_k| \parallel \boldsymbol{\gamma}_k \parallel_1 = \parallel \boldsymbol{x}_i^T\, \mathbf{B}^{-1} \parallel_1 \end{aligned}$$

Then, from (A2), it is apparent that $\lambda_{Ai} \leq 1 \; \forall i = 1, \ldots N$.

In conclusion, it has been shown that

$$0 < \lambda_{A1} \leq \lambda_{A2} \leq \ldots \leq \lambda_{A(N-1)} < \lambda_A^{max} = 1 \tag{A3}$$

Appendix B

In the remainder, inequality (14) is demonstrated assuming, for the sake of readability, the case with two DERs ($N = 2$). Expanding the matrix product $\mathbf{L}\,\bar{\boldsymbol{\epsilon}}$, it can be written

$$||\mathbf{L}\,\bar{\boldsymbol{\epsilon}}||_2^2 = ||\bar{\boldsymbol{\epsilon}}||_2^2 - \alpha_1\,\epsilon_1^2 - \alpha_2\,\epsilon_2^2 - 2\gamma\,\epsilon_1\epsilon_2 \tag{A4}$$

with

$$\alpha_i = 2\,a_{ii} - a_{ii}^2 - a_{ji}^2 \quad \text{for } i = 1,2 \text{ and } j \neq i \tag{A5}$$

$$\gamma = a_{12}(1 - a_{11}) + a_{21}(1 - a_{22}) \tag{A6}$$

Then, using (A4) it is trivial to verify that inequality (14) stands if

$$\alpha_1\,\epsilon_1^2 + \alpha_2\,\epsilon_2^2 + 2\gamma\,\epsilon_1\epsilon_2 > 0 \tag{A7}$$

Thanks to the properties of the elements of $\mathbf{A}$, it is $a_{ii} \geq a_{ji} > 0$ and $a_{ji} = 1 - a_{ii}$, for $i = 1,2$ and $j \neq i$. Consequently, from (A5), it can be written

$$\alpha_i \geq 2\,a_{ii} - 2\,a_{ii}^2 = 2\,a_{ii}a_{ji} \geq 2\,a_{ji}^2 > 0 \tag{A8}$$

and Equation (A6) becomes

$$\gamma = 2\,a_{12}\,a_{21} \tag{A9}$$

Using (A8) and (A9), the following sufficient conditions for inequality (A7) is derived

$$a_{12}^2\,\epsilon_1^2 + a_{21}^2\,\epsilon_2^2 + 2\,a_{12}\,a_{21}\,\epsilon_1\epsilon_2 > 0 \tag{A10}$$

which is always standing because the right-hand side is equal to $(a_{12}\,\epsilon_1 + a_{21}\,\epsilon_2)^2$. Indeed, inequality (A10) is not valid in a strict sense for the condition $a_{12}\,\epsilon_1 = -a_{21}\,\epsilon_2$. Nevertheless, substituting such a condition directly into the inequality (A7), it is trivially verified that (A7) stands in a strict sense.

References

1. Fusco, G.; Russo, M.; De Santis, M. Decentralized Voltage Control in Active Distribution Systems: Features and Open Issues. *Energies* **2021**, *14*, 2563. [CrossRef]
2. Carpinelli, G.; Di Fazio, A.; Perna, S.; Russo, A.; Russo, M. A-priori multi-objective optimization for the short-term dispatch of distributed energy resources. *Int. J. Electr. Power Energy Syst.* **2025**, *164*, 110410. [CrossRef]
3. Lv, Y.; Fu, J.; Wen, G.; Huang, T.; Yu, X. On consensus of multiagent systems with input saturation: Fully distributed adaptive antiwindup protocol design approach. *IEEE Trans. Control Netw. Syst.* **2020**, *7*, 1127–1139. [CrossRef]
4. Russo, A.; Incremona, G.P.; Seeber, R.; Ferrara, A. Adaptive Bounded Integral Control with Enhanced Anti-Windup Design. *IEEE Control Syst. Lett.* **2023**, *7*, 1861–1866. [CrossRef]
5. Xu, D.; Liu, J.; Yan, X.G.; Yan, W. A novel adaptive neural network constrained control for a multi-area interconnected power system with hybrid energy storage. *IEEE Trans. Ind. Electron.* **2017**, *65*, 6625–6634. [CrossRef]
6. Abdolmaleki, B.; Simpson-Porco, J.W.; Bergna-Diaz, G. Distributed optimization for reactive power sharing and stability of inverter-based resources under voltage limits. *IEEE Trans. Smart Grid* **2023**, *15*, 1289–1303. [CrossRef]
7. Qu, G.; Li, N. Optimal distributed feedback voltage control under limited reactive power. *IEEE Trans. Power Syst.* **2019**, *35*, 315–331. [CrossRef]
8. Da Silva, J.G.; Tarbouriech, S. Antiwindup design with guaranteed regions of stability: An LMI-based approach. *IEEE Trans. Autom. Control* **2005**, *50*, 106–111. [CrossRef]

9. Dehnert, R.; Lerch, S.; Tibken, B. Robust Anti Windup Controller Synthesis of Multivariable Discrete Systems with Actuator Saturation. In Proceedings of the 2020 IEEE Conference on Control Technology and Applications (CCTA), Montreal, QC, Canada, 24–26 August 2020; IEEE: New York, NY, USA, 2020; pp. 581–587.
10. Hencey, B.; Alleyne, A. An anti-windup technique for LMI regions. *Automatica* **2009**, *45*, 2344–2349. [CrossRef]
11. Ofodile, N.A.; Turner, M.C. Decentralized approaches to antiwindup design with application to quadrotor unmanned aerial vehicles. *IEEE Trans. Control Syst. Technol.* **2016**, *24*, 1980–1992. [CrossRef]
12. Ferrara, A.; Rubagotti, M. A sub-optimal second order sliding mode controller for systems with saturating actuators. *IEEE Trans. Autom. Control* **2009**, *54*, 1082–1087. [CrossRef]
13. Huang, S.; Xiong, L.; Zhou, Y.; Gao, F.; Jia, Q.; Li, X.; Li, X.; Wang, Z.; Khan, M.W. Distributed predefined-time control for power system with time delay and input saturation. *IEEE Trans. Power Syst.* **2024**, *40*, 151–165. [CrossRef]
14. Psillakis, H.; Alexandridis, A. Boundary layer sliding mode control for multimachine power systems improved by antiwindup integral action. In Proceedings of the 2005 International Conference on Control and Automation, Budapest, Hungary, 26–29 June 2005; IEEE: New York, NY, USA, 2005; Volume 1, pp. 497–502.
15. Xu, D.; Zhang, W.; Jiang, B.; Shi, P.; Wang, S. Directed-graph-observer-based model-free cooperative sliding mode control for distributed energy storage systems in DC microgrid. *IEEE Trans. Ind. Inform.* **2019**, *16*, 1224–1235. [CrossRef]
16. Antonelli, G.; Fusco, G.; Russo, M. Consensus-Based Model Predictive Control for Active Power and Voltage Regulation in Active Distribution Networks. *Energies* **2024**, *17*, 4490. [CrossRef]
17. Dar, M.R.; Ganguly, S. Voltage Regulation and Loss Minimization of Active Distribution Networks with Uncertainties Using Chance-Constrained Model Predictive Control. *IEEE Trans. Power Syst.* **2024**, *40*, 2737–2749. [CrossRef]
18. Escobar, E.D.; Betancur, D.; Manrique, T.; Isaac, I.A. Model predictive real-time architecture for secondary voltage control of microgrids. *Appl. Energy* **2023**, *345*, 121328. [CrossRef]
19. Li, S.; Wu, W. Data-Driven Linear-Time-Variant MPC Method for Voltage and Power Regulation in Active Distribution Networks. *IEEE Trans. Smart Grid* **2023**, *15*, 2625–2638. [CrossRef]
20. Yang, J.; Zhu, S.; Zhou, T. Distributed Model Predictive Control for Voltage Coordination of Distributed Photovoltaic Distribution Networks with High Permeability. *J. Appl. Sci. Eng.* **2025**, *28*, 1341–1350.
21. Hu, J.; Ye, C.; Ding, Y.; Tang, J.; Liu, S. A distributed MPC to exploit reactive power V2G for real-time voltage regulation in distribution networks. *IEEE Trans. Smart Grid* **2021**, *13*, 576–588. [CrossRef]
22. Karthikeyan, N.; Pillai, J.R.; Bak-Jensen, B.; Simpson-Porco, J.W. Predictive control of flexible resources for demand response in active distribution networks. *IEEE Trans. Power Syst.* **2019**, *34*, 2957–2969. [CrossRef]
23. Zhuang, K.; Xin, H.; Hu, P.; Wang, Z. Current saturation analysis and anti-windup control design of grid-forming voltage source converter. *IEEE Trans. Energy Convers.* **2022**, *37*, 2790–2802. [CrossRef]
24. Tong, X.; Zhao, X. Power Generation Control of a Monopile Hydrostatic Wind Turbine Using an H_∞ Loop-Shaping Torque Controller and an LPV Pitch Controller. *IEEE Trans. Control Syst. Technol.* **2017**, *26*, 2165–2172. [CrossRef]
25. Xiang, P.; Wang, X.; Mo, L. Cooperative H_∞ control of multiple high-speed trains with saturation constraints. *IEEE Access* **2019**, *7*, 129437–129442. [CrossRef]
26. Ästrom, K.J.; Hagglund, T. *Pid Controllers: Theory, Design and Tuning*; International Society of Automation, ISA: Durham, NC, USA, 1995.
27. Viswambharan, A.; Erouissi, R.; Shareef, H.; Stephen, S. A Robust Dynamic Compensator with Anti-windup Scheme for Grid-Interlinked Photovoltaic Inverter under Unbalanced Grid Voltages. In Proceedings of the IECON 2021—47th Annual Conference of the IEEE Industrial Electronics Society, Toronto, ON, Canada, 13–16 October 2021; IEEE: New York, NY, USA, 2021; pp. 1–6.
28. Baran, M.E.; Wu, F.F. Optimal capacitor placement on radial distribution systems. *IEEE Trans. Power Deliv.* **1989**, *4*, 725–734. [CrossRef]
29. Zhu, H.; Liu, H.J. Fast Local Voltage Control Under Limited Reactive Power: Optimality and Stability Analysis. *IEEE Trans. Power Syst.* **2016**, *31*, 3794–3803. [CrossRef]
30. Olfati-Saber, R.; Fax, J.A.; Murray, R.M. Consensus and Cooperation in Networked Multi-Agent Systems. *Proc. IEEE* **2007**, *95*, 215–233. [CrossRef]
31. IEEE DSA Subcommittee. IEEE PES Test Feeder. 1992. Available online: https://cmte.ieee.org/pes-testfeeders/ (accessed on 3 February 2025).
32. Fusco, G.; Russo, M. Local DER Control with Reduced Loop Interactions in Active Distribution Networks. *Energies* **2024**, *17*, 1991. [CrossRef]
33. Garin, F.; Schenato, L. A Survey on Distributed Estimation and Control Applications Using Linear Consensus Algorithms. In *Networked Control Systems*; Springer: London, UK, 2010; pp. 75–107. [CrossRef]

34. Millar, B.S.; Jiang, D. Asynchronous consensus for optimal power flow control in smart grid with zero power mismatch. *J. Mod. Power Syst. Clean Energy* **2018**, *6*, 412–422. .10.1007/s40565-018-0378-4. [CrossRef]
35. Golub, G.H.; Van Loan, C.F. *Matrix Computations*; JHU Press: Baltimore, MD, USA, 2013.